

¹ **Evaluation of New Snow Interception and
2 Canopy Snow Ablation Parameterisations for
3 Partitioning Snowfall in Needleleaf Forests**

⁴ Alex C. Cebulski¹, John W. Pomeroy¹ Bill C. Floyd^{2,3}

⁵ ¹Centre for Hydrology, University of Saskatchewan, Canmore, Canada

⁶ ²Ministry of Forests, Government of British Columbia, Nanaimo, British Columbia

⁷ ³Coastal Hydrology Research Lab, Vancouver Island University, Nanaimo, British Columbia

⁸ **Corresponding Author:** Alex C. Cebulski (alex.cebulski@usask.ca, ORCID ID - 0000-0001-
⁹ 7910-5056)

¹⁰ **Abstract**

¹¹ Snow falls in forests over 23% of the global land mass where snow interception and canopy snow
¹² ablation processes influence snow accumulation and land-surface energy exchanges. These pro-
¹³ cesses are strongly influenced by both meteorological conditions and canopy density, resulting
¹⁴ in differing process emergence in existing theories developed in distinctive climates, seasons,
¹⁵ and forest types, and limited transferability to new environments. Recent studies have re-
¹⁶ vealed new relationships to represent snow interception and canopy snow ablation processes
¹⁷ applicable across a broader range of canopy structures and climatic conditions. To assess the
¹⁸ effectiveness of these new parameterisations across differing climate and forests, both novel and
¹⁹ traditional routines were implemented in the Cold Regions Hydrological Modelling platform
²⁰ and evaluated against observations of canopy and subcanopy snow water equivalent across four
²¹ Canadian sites: two continental climate sites (Marmot Creek and Fortress Mountain, Alberta),
²² one subarctic site (Wolf Creek, Yukon Territory), and one temperate-maritime site (Russell

23 Creek, British Columbia). The observed fraction of seasonal snowfall stored in the subcanopy
24 snowpack at peak SWE varied from 0.3 at Russell Creek, 0.4 at Marmot and Wolf Creek, and
25 0.6 at Fortress Mountain. Uncalibrated simulation of canopy intercepted snow duration at
26 Marmot Creek improved with the new model, where the fractional differences from observa-
27 tions decreased from -40.1% to 10.2%. The new model demonstrated substantially improved
28 simulation of subcanopy snow accumulation, with mean bias dropping from -24.5 to -1.68 kg
29 m^{-2} across the four sites. At cold, low-wind sites, about half of annual snowfall was lost via sub-
30 limation of intercepted snow, whereas greater unloading at a colder, wind-exposed site reduced
31 sublimation losses. At the high-snowfall temperate maritime site, canopy snowmelt, meltwater
32 drip, and melt-induced unloading dominated, delivering the largest fraction of snowfall to the
33 forest floor despite high initial interception efficiency.

³⁴ **1 Introduction**

³⁵ Snow is an important water resource, directly supporting over two billion people globally
³⁶ (Immerzeel et al., 2020; Vivioli et al., 2020), while also affecting the Earth's energy balance
³⁷ via surface albedo (Thackeray et al., 2014; Wang et al., 2016), surface temperature (Pomeroy
³⁸ et al., 2016), soil temperature (Zhang et al., 2018), and stream temperatures (Leach & Moore,
³⁹ 2014). However, snowpacks are increasingly threatened due to changes in both climate and
⁴⁰ vegetation cover worldwide (Immerzeel et al., 2020; López-Moreno et al., 2014; Vivioli et al.,
⁴¹ 2020). Hydrological models are essential tools for understanding how climate and vegetation
⁴² influence snow processes and downstream water resources, and their accuracy depends on
⁴³ accurate representations of forest-snow processes. Snow falls in forested areas over half of
⁴⁴ the Northern Hemisphere (Kim et al., 2017) and over 23% of land mass globally (Deschamps-
⁴⁵ Berger et al., 2025), spanning diverse climates and forest structures, highlighting the need for
⁴⁶ robust, transferable models. In cold-dry climates, sublimation of snow intercepted by forest
⁴⁷ canopies can return up to 45% of seasonal snowfall back to the atmosphere (Essery et al.,
⁴⁸ 2003; Sanmiguel-Vallelado et al., 2017), whereas in temperate-maritime climates, sublimation
⁴⁹ is less prevalent and a large fraction of snowfall melts in the canopy (Storck et al., 2002).
⁵⁰ Yet, uncertainties in forest-snow process representation lead to variable transferability across
⁵¹ climates and forest types when simulating subcanopy snow water equivalent (SWE) (Essery
⁵² et al., 2003; Gelfan et al., 2004; Krinner et al., 2018; Rutter et al., 2009) and diagnosing snow
⁵³ processes (Lumbrazo et al., 2022; Lundquist et al., 2021). The strong dependence of snowfall
⁵⁴ partitioning on meteorology and canopy density compounds this variability (Mazzotti et al.,
⁵⁵ 2021; Pomeroy et al., 1998; Rojas-Heredia et al., 2024; Staines & Pomeroy, 2023; Storck et al.,
⁵⁶ 2002), challenging earlier canopy snow parameterisations developed from limited observations
⁵⁷ and leading to distinct process emergence across differing environmental conditions (Lundquist
⁵⁸ et al., 2021). While simulating SWE in forests remains challenging, it is a crucial aspect to
⁵⁹ understanding the impacts of climate and land cover changes on water resources in many
⁶⁰ forested cold regions across the globe.

61 Recent studies have advanced understanding of the canopy snow energy and mass balance
62 across a broader range in meteorological conditions and canopy structures (Cebulski &
63 Pomeroy, 2025b, 2025c; Lumbrazo et al., 2022; Lundquist et al., 2021; Mazzotti et al., 2021),
64 with potential to improve SWE simulations in more diverse forested basins. For example,
65 Lundquist et al. (2021) demonstrated that calculating throughfall as a function of antecedent
66 snow load can overestimate the amount of snow reaching the ground—when also combined
67 with a comprehensive canopy snow unloading routine. Building on this, Staines & Pomeroy
68 (2023) and Cebulski & Pomeroy (2025b) showed that initial interception can be predicted as a
69 function of canopy density without assuming a maximum canopy snow load. Moreover, Roesch
70 et al. (2001) and Lumbrazo et al. (2022) showed the importance of representing both wind
71 and melt-induced unloading for representing canopy snow ablation. A new physically-based
72 canopy snow mass and energy balance developed by Cebulski & Pomeroy (2025c) provided
73 improved representation of canopy snow ablation compared to previous approaches that were
74 either missing key processes such as dry snow unloading (Andreadis et al., 2009) or were
75 based on empirical relationships such as ice-bulb temperature indexed melt unloading and
76 drip (Ellis et al., 2010). These advances have been implemented as new parameterisations in
77 the modular Cold Regions Hydrological Modelling Platform (Pomeroy et al., 2022) to answer
78 the following research questions:

- 79 1. What is the fraction of seasonal snowfall stored in the subcanopy snowpack across forests
80 with differing climate and forest types?
 - 81 2. How accurately does a novel hydrological model simulate canopy snow load and sub-
82 canopy SWE across varying forest types and climates compared to an existing model?
 - 83 3. How is snowfall in needleleaf forests partitioned into interception, sublimation, unloading,
84 and melt/drip in differing climates and canopy structures?
- 85 The objective of this research is to evaluate new snow interception and ablation parameteri-
86 sations for simulating canopy and subcanopy SWE and to use the new parameterisations to
87 diagnose the role of these processes in partitioning snowfall and governing snow accumulation
88 under needleleaf forest canopies. Evaluation of the new model in simulating initial snow in-

89 interception has been addressed in Cebulski & Pomeroy (2025b) and canopy snow ablation in
90 Cebulski & Pomeroy (2025c).

91 **2 Methods**

92 **2.1 Study Sites**

93 The model evaluation was conducted at four locations in western and northern Canada span-
94 ning a range of climate and forest types (Fig. 1; Table 1). The model simulation years for
95 each site are shown in Table 1 and were selected based on the availability of subcanopy SWE
96 measurements and hourly station-based observations of air temperature, relative humidity,
97 wind speed, total precipitation, and net solar radiation adjacent to the snow survey transects.
98 At each site, snow surveys consisted of snow depth measurements at all locations and snow
99 density measurements at one out of every five locations. SWE was calculated from snow depth
100 and snow density following the methods outlined in Pomeroy & Gray (1995). The four study
101 sites include:

102 Wolf Creek Research Basin - Forest Site (60.60°N , 134.96°W , 750 m asl.) is located 16 km
103 south of Whitehorse, Yukon Territory in a level dense forest with a sub-arctic climate (see
104 basin scale location in Fig. 1 in Rasouli et al., 2019). Snow surveys were conducted along
105 a transect that traverses through mature forest consisting of primarily white spruce (*Picea*
106 *glauca*) and interior Lodgepole pine (*Pinus contorta*). Additional details on the snow survey
107 and meteorological measurements is described in Rasouli et al. (2019).

108 Russell Creek Experimental Watershed - Upper Stephanie Old Growth Site (50.32°N ,
109 126.35°W , 700 m asl.) is located on northern Vancouver Island, British Columbia (Fig. 1) in
110 a temperate-maritime climate that receives substantial precipitation (>2000 mm/yr, Fig. 2).
111 Snow survey transects were conducted in cardinal directions within a mature old growth
112 forest that consists of Amabilis fir (*Abies amabilis*) and western hemlock (*Tsuga heterophylla*)
113 (Floyd, 2012). Additional details on the snow survey and meteorological instrumentation

114 are provided in Floyd (2012). Total precipitation data were unavailable at the Russell site
115 for the 2008 water year. For this period, records from the Tsitika Summit station (50.28°N,
116 126.36°W; 450 m asl.), operated by the British Columbia Ministry of Transport and located 5
117 km from Russell, were used instead.

118 Fortress Mountain Research Basin - Powerline site (50.83°N, 115.20°W, 2100 m asl.,
119 Kananaskis, Alberta) is located on a wind-exposed subalpine ridge top covered with sparse
120 forest with a continental climate (Fig. 1). The vegetation at this site consists of coexisting
121 mature subalpine fir (*Abies lasiocarpa*) and Engelmann spruce (*Picea engelmannii*) tree
122 species (Langs et al., 2020). Snow survey measurements of snow depth and density were
123 collected following a transect through mature forest east of the Powerline meteorological
124 tower (see Fig. 1 in Cebulski & Pomeroy, 2025b). The meteorological forcing data used in
125 this study is described in detail in Cebulski & Pomeroy (2025c). An evaluation of the new
126 canopy snow model on canopy snow load observations was presented in Cebulski & Pomeroy
127 (2025b) and Cebulski & Pomeroy (2025c) at Fortress Mountain.

128 Marmot Creek Research Basin - Upper Forest site (50.93°N, 115.16°W, 1848 m asl., Kananaskis,
129 Alberta) is located on a dense forested plateau with a continental climate 14 km north of
130 Fortress (see basin scale location in Fig. 1 in Fang et al., 2019) but receives much less pre-
131 cipitation (Fig. 2). The forest consists primarily of Engelmann spruce (*Picea engelmannii*),
132 subalpine fir (*Abies lasiocarpa*), and Lodgepole pine (*Pinus contorta*) species (Fang et al., 2019;
133 Staines & Pomeroy, 2023). Snow surveys were conducted following a cardinal transect through
134 mature forest surrounding the “Upper Clearing” meteorological tower (see Fig. 1b in Staines
135 & Pomeroy, 2023). The meteorological forcing data and corresponding instrumentation used
136 from this site are described in Fang et al. (2019). Canopy snow load observations were col-
137 lected within the Upper Forest to validate simulations. A weighed subcanopy snow bucket
138 installed by MacDonald (2010) provided throughfall measurements, which were used with a
139 mass balance calculation (Eq. 5 in Cebulski & Pomeroy, 2025a) to estimate canopy snow load
140 for 11 snowfall events between February 2007 and February 2008. A weighed tree lysimeter
141 installed by Staines (2021) on the Upper Forest meteorological tower provided measurements

¹⁴² of snow load between December 2018 and June 2019. The weighed tree was scaled from weight
¹⁴³ of intercepted snow in the tree to mass of intercepted snow per unit area using snow survey
¹⁴⁴ measurements from the two snowfall events reported in Staines & Pomeroy (2023) following
¹⁴⁵ the methodology outlined in Pomeroy & Schmidt (1993) and Hedstrom & Pomeroy (1998).

Table 1: Simulation period (Years), location, and vegetation characteristics, including canopy cover (C_c), leaf area index (LAI), and mean tree height (\bar{h}_t), for the four study sites.

Site Name	Years	Elevation (m)	Latitude (°N)	Longitude (°W)	C_c (-)	LAI (-)	\bar{h}_t (m)	Dominant Species
Wolf Creek	2015– 2022	750	60.60	134.96	0.81	3.82	15.0	White Spruce and interior lodgepole pine
Marmot Creek	2006– 2023	1848	50.93	115.16	0.80	3.00	15.0	Engelmann spruce, subalpine fir, and lodgepole pine
Fortress Mountain	2013– 2023	2100	50.83	115.20	0.65	1.44	10.5	Subalpine fir and engelmann spruce
Russell Creek	2006– 2008	700	50.32	126.35	0.86	1.93	44.9	Amabilis fir and western hemlock

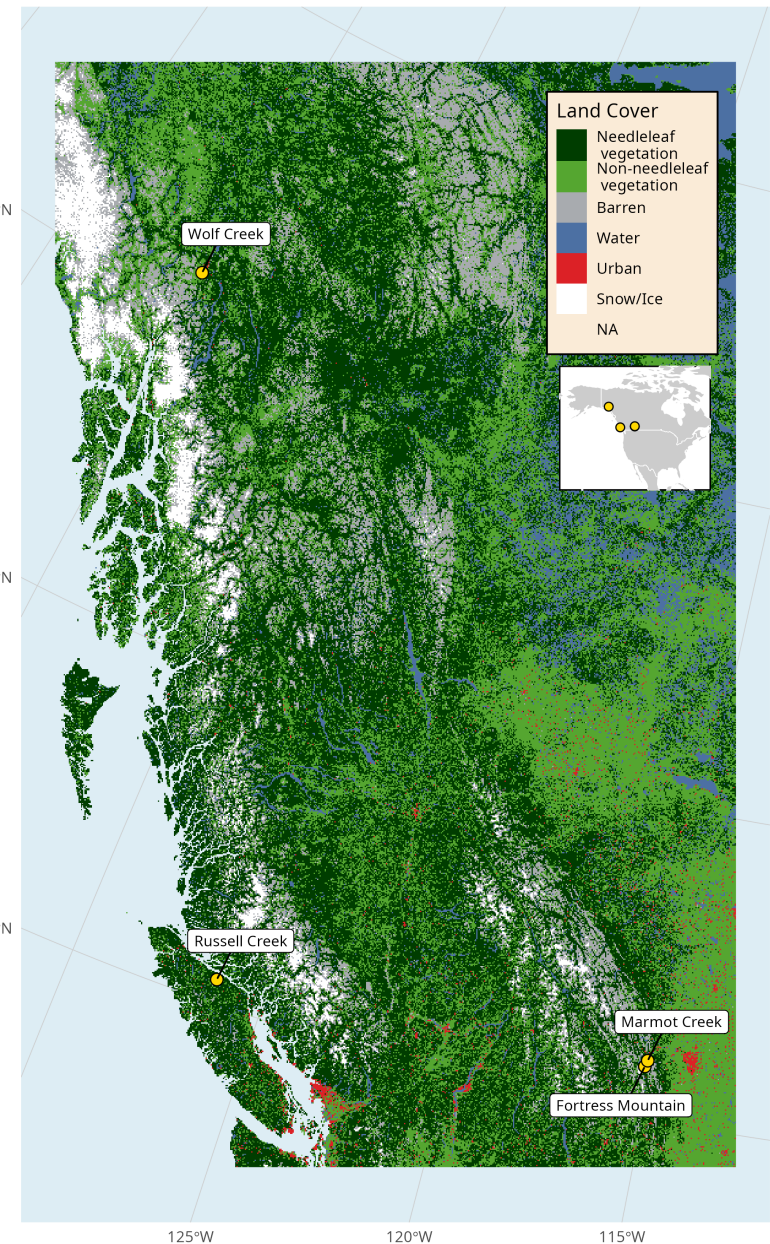


Figure 1: Map showing the regional scale location of the four research basins and land cover data from the Canada Centre for Remote Sensing, Canada Centre for Mapping and Earth Observation & Natural Resources Canada (2020) North American Land Change Monitoring 30-metre dataset.

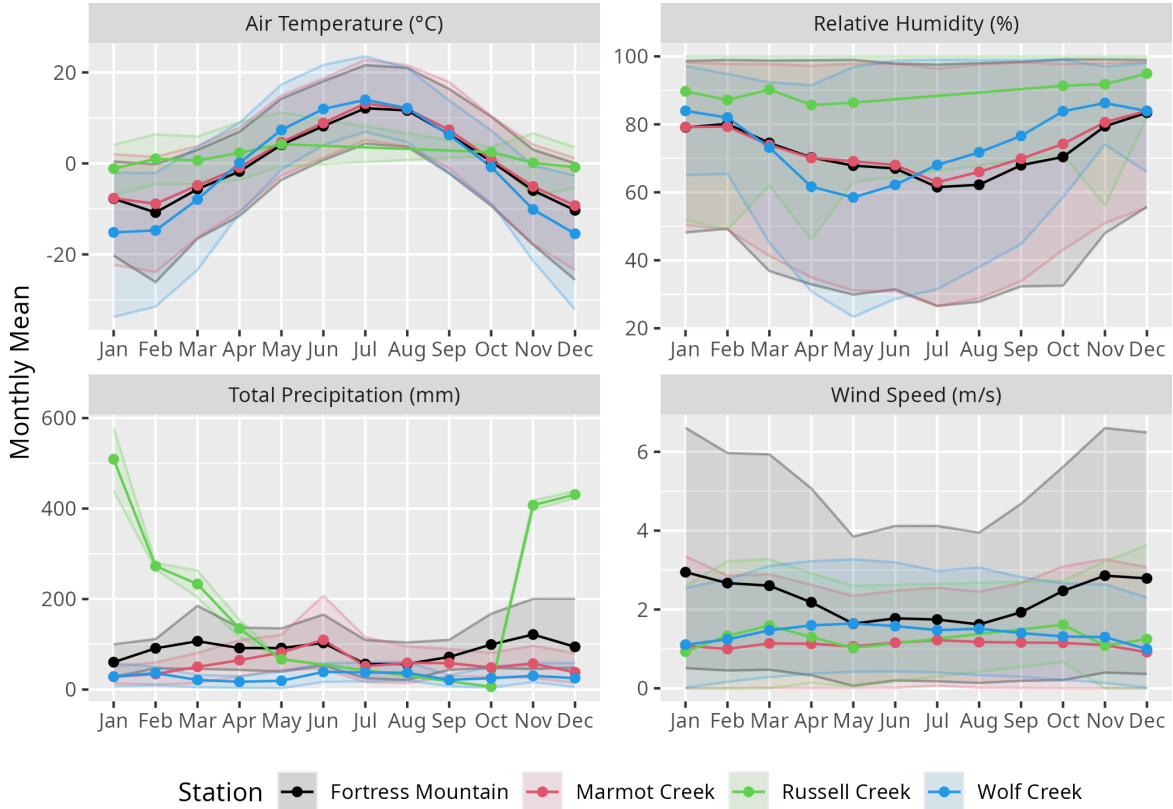


Figure 2: Mean monthly relative humidity, air temperature, total precipitation, and wind speed at each station over the simulation period. Points and solid lines indicate monthly means, while the shaded band represents the 5th–95th percentile range across the corresponding years for each site (see Table 1 for station metadata). Observations were not available during the snow free period for Russell Creek (Jun to Sept). Wind speeds are reported for above-canopy conditions.

¹⁴⁶ 2.2 Simulation of Subcanopy Snowpack

¹⁴⁷ The Cold Regions Hydrological Modelling Platform (CRHM) was implemented to simulate
¹⁴⁸ SWE stored in the canopy and in the subcanopy snowpack, and diagnose processes that
¹⁴⁹ partition intercepted snow at each of the four forest plots. The CRHM platform is de-
¹⁵⁰ scribed in detail by Pomeroy et al. (2022). The up-to-date source code is available at
¹⁵¹ <https://github.com/srlabUsask/crhmcode>, and the version used in this manuscript is archived

152 at Pomeroy et al. (2025). Hourly climate forcing data from station-based measurements of air
153 temperature, relative humidity, wind speed, total precipitation, and above canopy incoming
154 solar radiation were used to run the CRHM models. Incoming solar radiation observations
155 were not available for Wolf Creek and were simulated following theoretical clear-sky radiation
156 by Garnier & Ohmura (1970) and atmospheric transmittance by Shook & Pomeroy (2011)
157 using an adaptation of the method developed by Annandale et al. (2002).

158 Precipitation phase was determined following the psychrometric energy balance approach of
159 Harder & Pomeroy (2013) which accounts for the influence of temperature and humidity on
160 precipitation phase. The canopy snow mass and energy balance was treated using two dif-
161 ferent approaches. An updated approach following new relationships presented in Cebulski
162 & Pomeroy (2025b) and Cebulski & Pomeroy (2025c) hereafter called “CP25” to represent
163 the canopy snow energy and mass balance (see Supporting Information for a description of
164 the changes to CRHM to implement the new CP25 model). This new approach simulates
165 initial interception of snow in the canopy as a function of canopy density and hydrometeor
166 trajectory angle (Cebulski & Pomeroy, 2025b) and subsequent ablation of snow intercepted
167 in the canopy by melt and dry-snow unloading (Cebulski & Pomeroy, 2025c), energy balance-
168 based snowmelt (Cebulski & Pomeroy, 2025c), and energy balance-based sublimation (Essery
169 et al., 2003). The terminal fall velocity of hydrometeors used in the initial snow interception
170 parameterisation was assumed to be constant at 0.8 m s^{-1} , based on observations reported
171 in Cebulski & Pomeroy (2025b) and Isyumov (1971). The shear stress used in the canopy
172 snow unloading parameterisation was approximated as the square of wind speed multiplied
173 by an empirically derived correction factor which was obtained from observations at Fortress
174 Mountain presented in Cebulski & Pomeroy (2025c). A second approach hereafter called “E10”
175 which is based on observations by Hedstrom & Pomeroy (1998), Pomeroy et al. (1998), and
176 Floyd (2012); and implemented as described in Ellis et al. (2010). E10 calculates initial inter-
177 ception of snow in the canopy as a function of canopy density, antecedent snow load, and a
178 species dependent storage capacity following Hedstrom & Pomeroy (1998). Ablation of snow
179 intercepted in the canopy is determined by dry snow unloading (function of canopy snow load

as in Hedstrom & Pomeroy, 1998), unloading due to melt (Ellis et al., 2010), canopy snowmelt drainage (threshold function of ice-bulb temperature as in Ellis et al., 2010), and sublimation by an analytical energy balance-based parameterisation (Pomeroy et al., 1998). See Cebulski & Pomeroy (2025a) for a complete description of the E10 parameterisation. While neither the E10 nor CP25 model was calibrated for this study, their parameterisations were originally developed using data from Marmot and sites in Prince Albert National Park, northern Saskatchewan (E10) and Fortress (CP25).

A two-layer energy and mass balance snowmelt model (Snobal, Marks et al., 1998) was used to calculate subcanopy snowpack evolution. Net shortwave radiation to the subcanopy snowpack was simulated by calculating the transmittance of irradiance through the canopy, less the amount reflected from the snow surface (Ellis et al., 2010; Pomeroy et al., 2008). Incoming longwave radiation to subcanopy snow was simulated by thermal emissions from the atmosphere and vegetation elements, weighted by sky-view-factor (Ellis et al., 2010; Pomeroy et al., 2009). Sensible and latent heat fluxes to the subcanopy snowpack were determined using an approach adopted from Brutsaert (1982) and Marks & Dozier (1992) and is described in the CRHM source code. Only two water years were simulated at Russell due to limited model forcing and validation data.

2.3 Model Evaluation

Simulated canopy snow load at Marmot Creek and subcanopy SWE at the four forest plots by the two models (E10 and CP25) was evaluated using observations. The performance of the two models was evaluated based on the differences in simulated (S_i) and observed (O_i) values of SWE using mean bias (MB), root mean squared error (RMSE), Nash-Sutcliffe efficiency (NSE, Nash & Sutcliffe, 1970), and Kling-Gupta Efficiency (KGE, Gupta et al., 2009; Clark et al., 2021) as:

$$MB = \frac{1}{n} \sum_{i=1}^n (S_i - O_i) \quad (1)$$

$$\text{RMSE} = \sqrt{\frac{\sum_{i=1}^n (S_i - O_i)^2}{n}} \quad (2)$$

$$\text{NSE} = 1 - \frac{\sum_{i=1}^n (S_i - O_i)^2}{\sum_{i=1}^n (O_i - \bar{O})^2} \quad (3)$$

$$\text{KGE} = 1 - \sqrt{\left(\frac{\bar{S}}{\bar{O}} - 1\right)^2 + (\alpha - 1)^2 + (\rho_p - 1)^2} \quad (4)$$

where \bar{O} and \bar{S} are the means of the observed and simulated values, respectively, n is the number of observations, α is the ratio of simulated to observed standard deviation, and ρ_p is the Pearson correlation the simulated and observed values.

Performance metrics were calculated over the full simulation period using all available observations of canopy snow load and subcanopy SWE at each site. To quantify sampling uncertainty associated with the inclusion of potentially influential observations, a bootstrap resampling procedure with replacement (10 000 bootstrap replicates) was applied (Clark et al., 2021). For the canopy snow load evaluation, snowfall events with observed snow load greater than 1 mm ($n = 18$) were treated as resampling blocks. For the subcanopy SWE evaluation, individual snow survey observations were used as resampling blocks, due to their low temporal autocorrelation resulting from biweekly or monthly sampling intervals.

3 Results

3.1 Snowpack Observations

Amongst the sites and years included in the study, accumulation of snowfall below the canopy was less than cumulative snowfall observed in open clearings adjacent to each forest transect (Fig. 3). At peak seasonal subcanopy SWE, Fortress had the highest fraction of seasonal

220 snowfall stored in the subcanopy snowpack at 0.6, followed by Marmot and Wolf Creek which
221 both had similar fractions at 0.4, and Russell had the smallest fraction at 0.3—when averaged
222 over all years. The variability across years was highest at Wolf Creek ranging from 0.2 to
223 0.6 (Fig. 4). Fortress and Marmot Creek also exhibited substantial variability across years
224 (Fig. 4). In contrast, Russell Creek showed the least variation; however, this assessment is
225 limited by observations from only two winter seasons (Fig. 4). Differences in partitioning of
226 intercepted snow by canopy snow unloading, melt/drip, and sublimation contributed to the
227 observed differences in subcanopy snow accumulation relative to the open clearings across sites
228 and years. At the temperate-maritime Russell site, mid-winter melt events also contributed
229 to these observed differences. Section 3.5 presents a diagnosis of the dominant processes that
230 partitioned snowfall across the four different forest plots leading to the observed differences in
231 subcanopy snow accumulation.

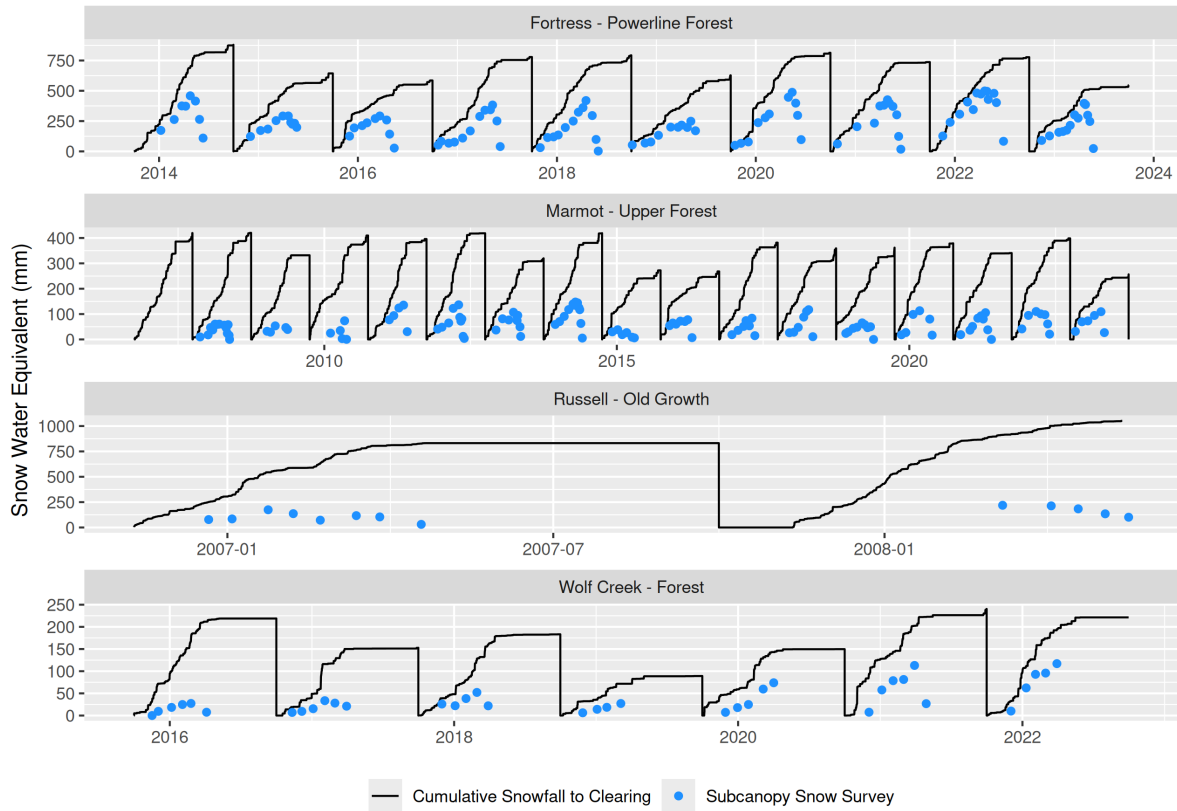


Figure 3: Time series showing seasonal cumulative snowfall (black lines) and subcanopy SWE from snow surveys (blue dots). Note: snowfall was determined from observed total precipitation to an open clearing for each site using the snowfall fraction simulated in CRHM following Harder & Pomeroy (2013).

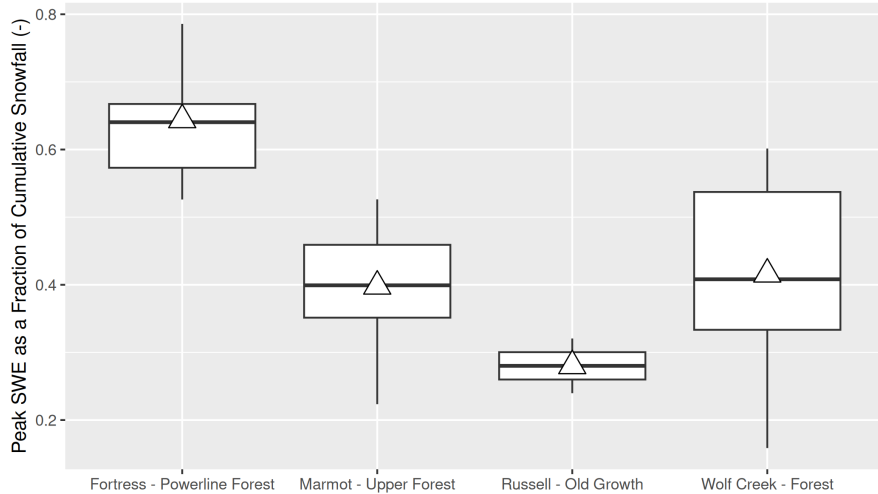


Figure 4: Boxplots showing peak SWE as a fraction of cumulative snowfall. Subcanopy SWE observations are from snow surveys and snowfall was determined from observed total precipitation to an open clearing for each site using the snowfall fraction simulated in CRHM following Harder & Pomeroy (2013). Note: the rectangle vertical extent represents the interquartile range (25th to 75th percentile), the horizontal line within each box indicates the median, and the whiskers extend to 1.5 times the interquartile range. The white triangle denotes the mean across all years.

232 3.2 Canopy Snow Load Evaluation

233 Canopy snow load was overestimated by CP25 and underestimated by E10, over the two
 234 observation periods between February 2007–February 2008 and December 2018–June 2019 at
 235 Marmot Creek (Fig. 5). The error in simulated canopy snow load over the two periods was
 236 smaller for CP25 with a mean bias of -0.4 kg m^{-2} compared to the E10 mean bias of 1 kg m^{-2}
 237 (Table 2). The CP25 model also produced higher NSE (0.83) and KGE (0.73) values compared
 238 to E10, which had lower NSE (0.6) and KGE (0.33) values. CP25 demonstrated improved
 239 accuracy across a range of snow loads, while E10 greatly underestimated larger snow loads,
 240 as above the species specific canopy holding capacity the E10 model decreases the fraction
 241 of new snow that is intercepted in the canopy (Fig. 5). Results from the bootstrap analysis,
 242 which resampled different combinations of the 18 canopy snowfall events at Marmot Creek,
 243 quantified the sampling uncertainty associated with event selection. Across the resampled

datasets, the CP25 model more accurately simulated canopy snow load, as indicated by its higher KGE value (0.67) relative to the poorer performance of E10 (0.3) (Fig. 6). The E10 model consistently underestimated canopy snow load, as shown by a positive mean bias across all event combinations. In contrast, CP25 exhibited a smaller negative mean bias that was closer to zero, although it also underestimated snow load for some event combinations, as indicated by the positive upper bound of the 95% confidence interval.

For five events between May and June 2019, characterised by mean air temperatures above 0°C with mixed snowfall and rainfall, canopy snow load was underestimated by both CP25 and E10 (see Supporting Information for a subset of Fig. 5 for just these events). Two precipitation events (2019-05-30 and 2019-06-14) were simulated by CRHM entirely as rain. During these events, observed canopy loads reached 2.6–3.0 kg m⁻², indicative of snow interception, whereas simulated loads were < 0.5 kg m⁻², close to the liquid storage capacity used in both CP25 and E10. For the remaining three events with mixed snow/rain on 2019-05-15, 2019-05-23, and 2019-06-06 CP25 underestimated peak canopy snow load by -18.1% to -84.4% and E10 by -54.7% to -69.4%. The underestimation of simulated canopy load by both models over these events is attributed to the liquid storage capacities of canopy snow and vegetation elements, not representing differing unloading rates with increased cohesion/adhesion of snow to the canopy near the melting point, instrument uncertainty in the observations, and errors in the precipitation phase parameterisation.

Over the 2018–2019 period the fraction of the year that the canopy was loaded with >2 kg m⁻² of snow, was found to be 0.26, compared to simulations of 0.29 and 0.16 by the CP25 and E10 models respectively. A threshold of 2 kg m⁻² was selected based on observations by Pomeroy & Dion (1996) who found minimal influence of canopy snow load on above canopy albedo for loads less than 1.6 kg m⁻². The underestimate of canopy intercepted snow duration by the E10 model of around -40.1% results from the underestimation of canopy load which depleted the canopy of snow earlier than the observations. The CP25 model slightly overestimated the intercepted snow duration by 10.2%, resulting from the overestimates of canopy snow load by CP25 (Fig. 5) which stored canopy snow loads above >2 kg m⁻² longer than the observations.

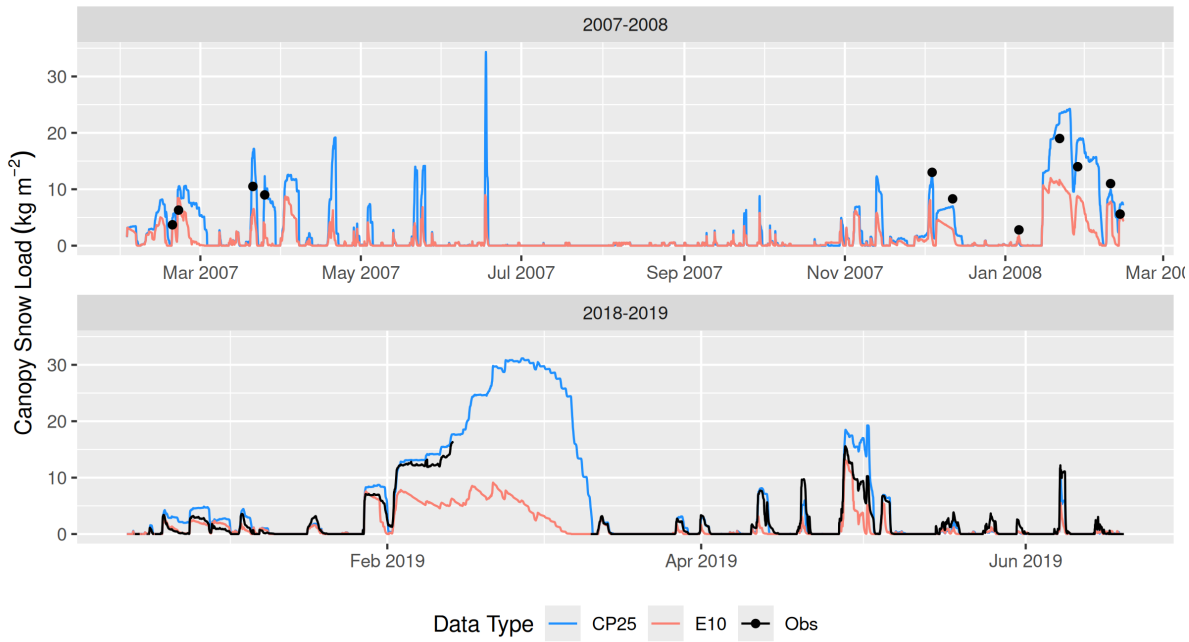


Figure 5: Timeseries of observed and simulated (CP25 and E10) canopy snow load at Marmot Creek for two periods February 2007 to February 2008 (top) and December 2018 to June 2019 (bottom).

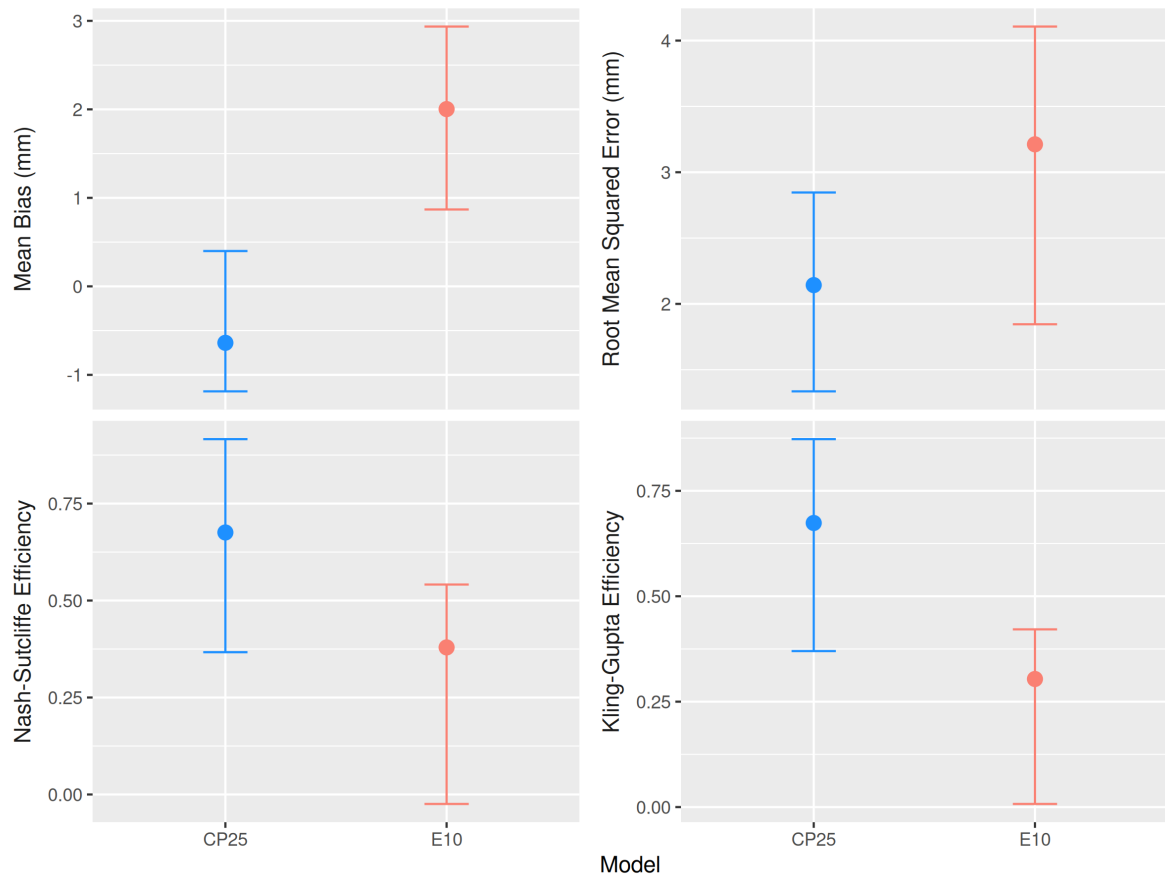


Figure 6: Error statistics derived from bootstrap resampling of differing combinations of canopy snow load events (10 000 replicates) at Marmot Creek between December 2018 and June 2019. Points indicate the mean metric, and error bars show the 95% confidence intervals estimated across all resampled event combinations.

Table 2: Mean bias (MB), root mean squared error (RMSE), Nash-Sutcliffe efficiency (NSE), and Kling-Gupta efficiency (KGE) determined from time-series simulations of canopy snow load for the two models CP25 and E10 at Marmot Creek. The final column (n) shows the count of observations used to compute the statistics.

Model	Year	MB	RMSE	NSE	KGE	n
CP25	2007-2008	-1.93	3.26	0.50	0.60	11
E10	2007-2008	3.82	5.30	-0.33	0.35	11
CP25	2018-2019	-0.37	1.58	0.83	0.73	3838
E10	2018-2019	1.03	2.39	0.60	0.33	3838
CP25	All	-0.37	1.59	0.83	0.73	3849
E10	All	1.04	2.40	0.60	0.33	3849

272 3.3 Subcanopy Snowpack Evaluation

273 Over all years and sites, the CP25 model had a lower mean bias of -1.68 kg m^{-2} compared
 274 to E10's mean bias of -24.5 kg m^{-2} in representing subcanopy SWE measurements (Table 3).
 275 Model errors were lower for the three colder climate sites (i.e., Fortress, Marmot, and Wolf
 276 Creek), where CP25 underestimated SWE ($\text{MB} = 2.87 \text{ kg m}^{-2}$) and E10 overestimated SWE
 277 ($\text{MB} = -9.99 \text{ kg m}^{-2}$). Although E10 had a marginally reduced mean bias at Fortress compared
 278 to CP25, the RMSE, NSE, and KGE values were improved across all sites for CP25 reflecting
 279 improved accuracy of the new model (Table 3). Three years contributed to the higher RMSE
 280 and lower NSE and KGE values by E10 at Marmot where simulated peak SWE was greatly
 281 overestimated by over 50 kg m^{-2} (nearly 100% of observed SWE) for the water years 2011 and
 282 2012. In contrast, E10 had a very large underestimation in subcanopy SWE at Marmot for the
 283 water year 2019. At Wolf Creek, E10 also had deviations of $\sim 30 \text{ kg m}^{-2}$ ($\sim 100\%$ greater than
 284 observed SWE) from peak SWE for 2016 and 2017. At Russell Creek, errors were lower for both
 285 CP25 and E10 during the first winter season than the second. This difference may be explained
 286 by a higher frequency of cold snowfall events during the first year, when air temperatures

frequently dropped below -10°C , compared with the second year when temperatures did not fall below -8°C . The colder conditions in the first year were more consistent with those at Fortress Mountain, where the CP25 parameterisations were developed. In contrast, the relatively warmer second winter could have promoted stronger melt-freeze processes, resulting in more cohesive canopy snow, greater canopy retention, and reduced partitioning into solid snow unloading. Although the intent of this evaluation is to assess the performance of each model in simulating subcanopy SWE, uncertainties in model forcing and physical parameters (i.e., canopy coverage, LAI) may also contribute to systematic biases in the evaluation. Some of the increased model error at Russell during the 2008 water year may reflect the use of total precipitation data from a nearby highway station rather than on-site measurements.

Bootstrap resampling revealed clear differences in model performance in simulating subcanopy snow water equivalent (SWE) across the evaluated sites (Fig. 8, Fig. 9). The CP25 model had consistently lower RMSE, KGE, and NSE mean values, as well as a smaller 95% confidence interval, across all four sites. The mean bias statistic differed less between the two models with E10 showing a slightly lower mean bias at Fortress, versus lower mean bias for CP25 at Marmot. Still, the range in mean biases across the differing event combinations for CP25 was smaller showing more stable performance. Across the three cold climate sites (Fortress, Marmot, and Wolf Creek) the greatest deviation in the error statistics between the two models was observed at Marmot Creek, with improved accuracy for the CP25 model and less difference in performance at Fortress and Wolf Creek. Both CP25 and E10 had higher errors at Russell Creek compared to the colder climate sites, though CP25 still had substantially greater accuracy compared to CP25 due to a better representation of canopy snow ablation processes (Fig. 9).

Table 3: Mean bias (MB), root mean squared error (RMSE), Nash-Sutcliffe efficiency (NSE), and Kling-Gupta efficiency (KGE) determined from time-series simulations of snow water equivalent for the two canopy snow models at each of the four sites. The final column (n) shows the count of observations used to compute the statistics.

Model	Station	MB	RMSE	NSE	KGE	n
CP25	All Station Mean	-1.68	45.8	0.86	0.92	282
E10	All Station Mean	-24.54	110.3	0.20	0.55	282
CP25	Fortress - Powerline	5.10	43.8	0.89	0.94	109
	Forest					
E10	Fortress - Powerline	-4.58	52.2	0.84	0.90	109
	Forest					
CP25	Marmot - Upper Forest	2.29	20.9	0.69	0.79	124
E10	Marmot - Upper Forest	-5.02	30.6	0.33	0.62	124
CP25	Russell - Old Growth	-127.40	162.7	-7.24	-0.95	12
E10	Russell - Old Growth	-465.37	500.0	-76.80	-3.63	12
CP25	Wolf Creek - Forest	5.78	17.4	0.70	0.75	37
E10	Wolf Creek - Forest	-5.81	21.9	0.52	0.71	37

310 The evolution of season subcanopy SWE was generally represented well by both models at
 311 Fortress, Marmot, and Wolf Creek (Fig. 7). However, E10 failed to simulate the timing
 312 of SWE accumulation and ablation well for 2011, 2012, and 2019 at Marmot. The largest
 313 deviation in simulated seasonal SWE occurred at Russell Creek for E10 where subcanopy snow
 314 accumulation was simulated at a much higher rate compared to that observed and estimated by
 315 CP25 over the two years that were simulated. At Wolf Creek, CP25 had a delay in simulating
 316 the initial accumulation of subcanopy SWE for water years 2017, 2018, and 2019. The lower
 317 snowfall rate at Wolf Creek and higher interception rate for CP25 compared to E10 led to
 318 throughfall and unloading rates that were smaller than the snowpack initiation threshold
 319 employed in Snobal, causing simulated SWE below this threshold to melt immediately. In

320 contrast, E10 intercepted less snow and had higher unloading rates than CP25 leading to
 321 higher initial accumulation for these three years at Wolf Creek.

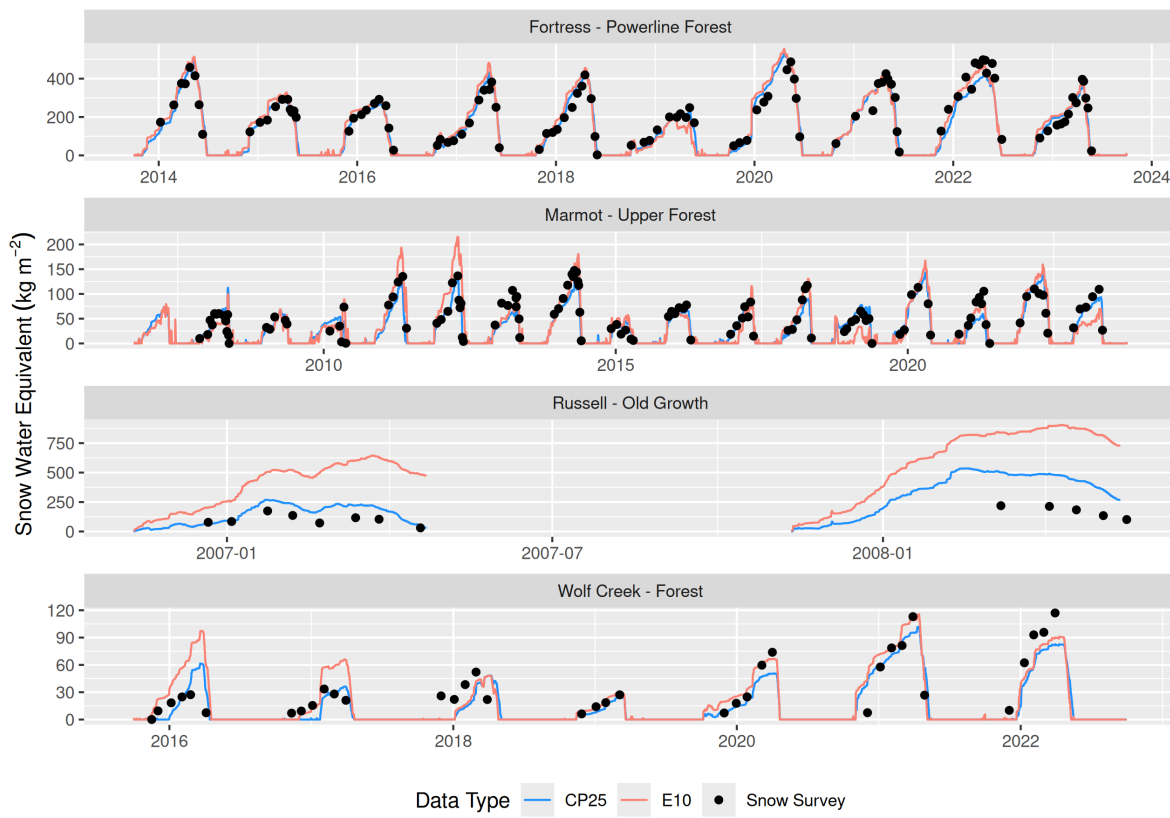


Figure 7: Timeseries of observed and simulated (CP25 and E10) forest snow water equivalent at each station.

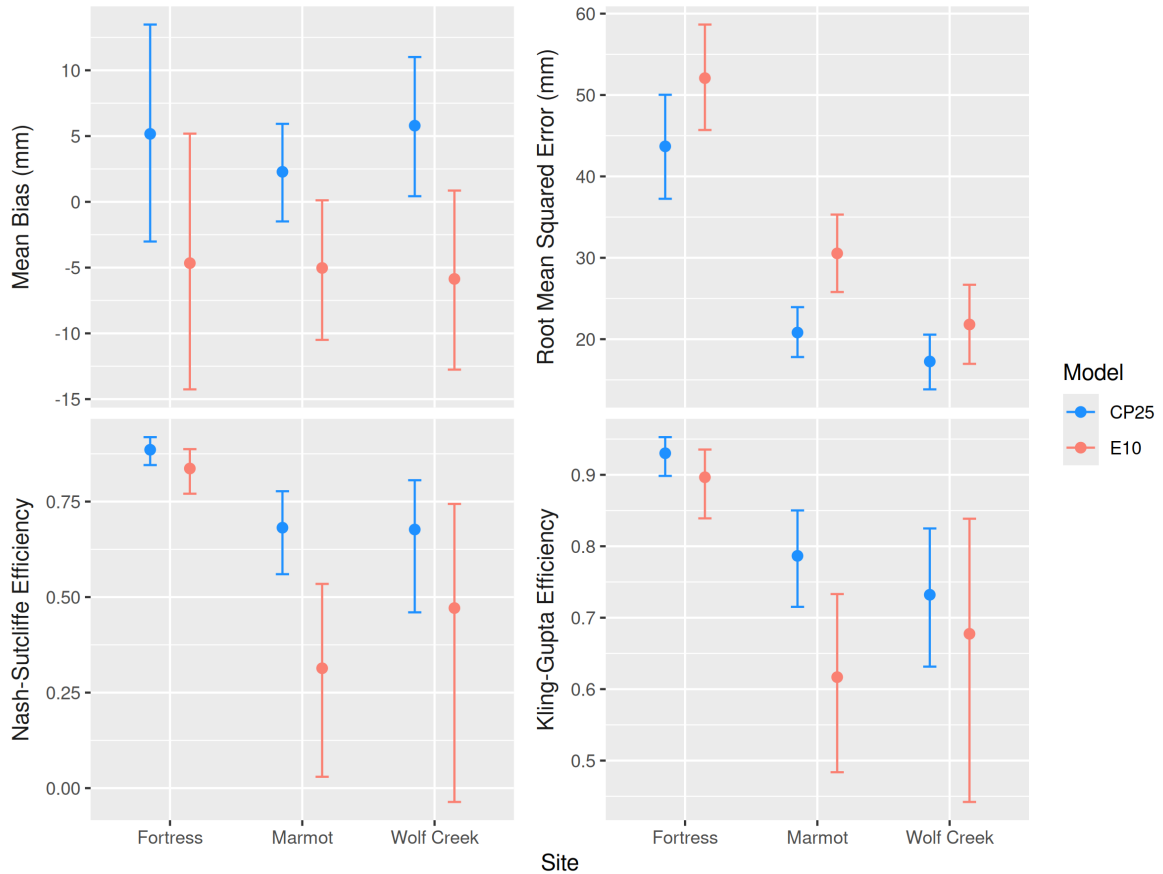


Figure 8: Error statistics from bootstrap resampling of differing combinations of subcanopy SWE measurements (10 000 replicates) at Fortress Mountain, Marmot Creek, and Wolf Creek. Russell Creek is shown in Fig. 9 due to the differing magnitude of error. Points indicate the mean metric and error bars show the 95% confidence intervals estimated across all resampled event combinations.

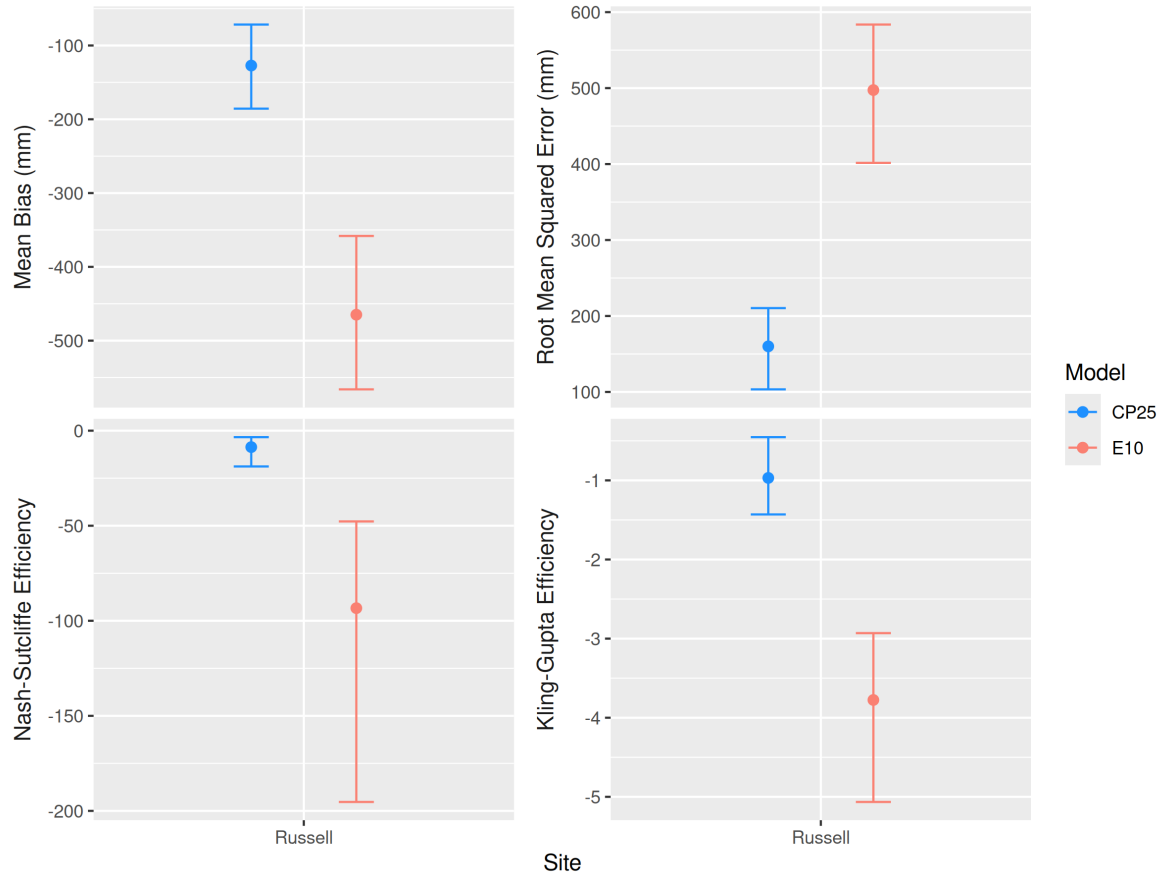


Figure 9: Error statistics from bootstrap resampling of differing combinations of snow surveys (10 000 replicates) at Russell Creek. Points indicate the mean metric and error bars show the 95% confidence intervals estimated across all resampled event combinations.

322 **3.4 Simulated Canopy Snow Load**

323 Over all years and sites, CP25 predicted consistently higher canopy snow loads compared
324 to the E10 model (Fig. 10). This was due to E10's increase in throughfall with increasing
325 antecedent snow load as well as the unloading rate as a function of snow load and ice-bulb
326 temperature which led to increased throughfall and unloading for E10 and less snow residing
327 in the canopy compared to CP25. Some snowfall events had similar initial accumulation of
328 snow in the canopy between the two models up until the E10 species snow load capacity was
329 reached (see events in Jan and Feb at Fortress, Marmot, and Wolf Creek in the Supporting
330 Information).

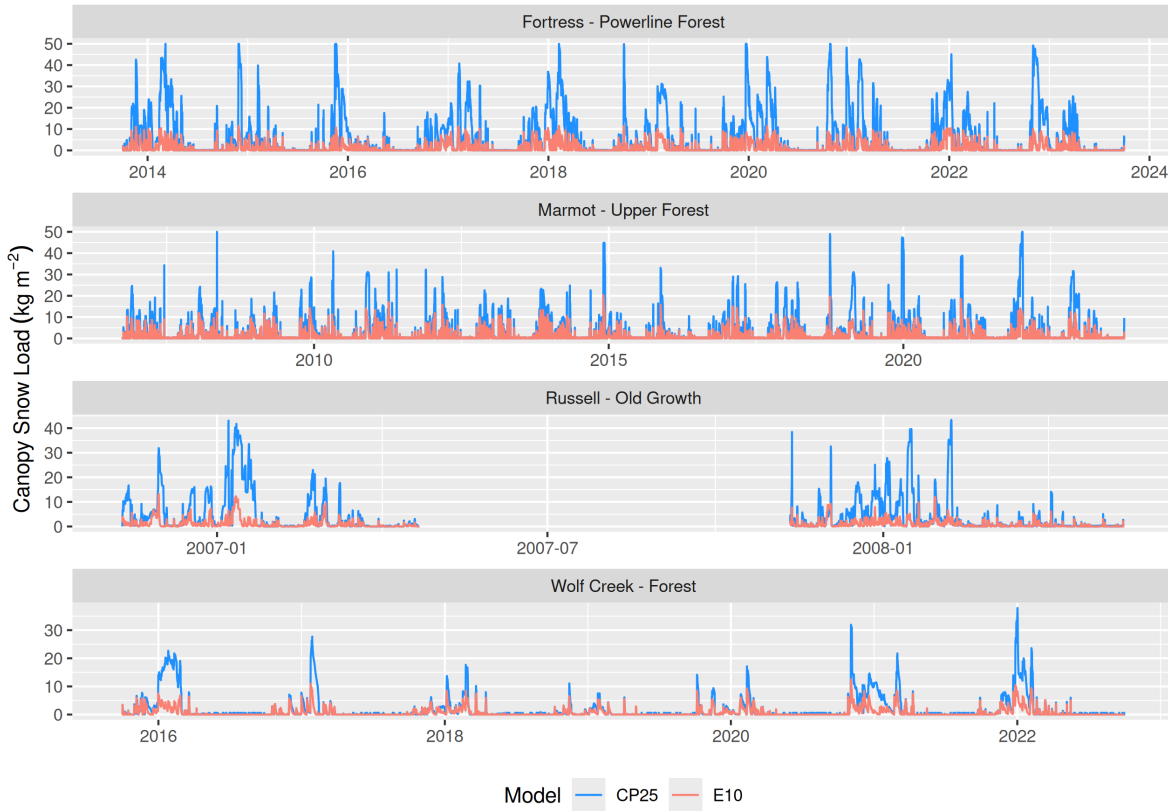


Figure 10: Timeseries of simulated canopy load for CP25 and E10 at each station for the full simulation period.

331 In addition to the large difference in canopy snow load predicted by CP25 and E10 across
 332 all four sites, the duration that the canopies of each site were simulated to have more than 2
 333 kg m⁻² of snow varied between the four sites and two models (Fig. 11). Across all four sites,
 334 canopy snow loads greater than 2 kg m⁻² were observed to persist longer for CP25 compared
 335 to E10 (Fig. 11). The largest differences between the two models occurred at Russell and
 336 Fortress, where snow loads exceeding this threshold persisted 131% and 75% longer in CP25
 337 than in E10. At Marmot and Wolf Creek, the relative differences were smaller—61% and
 338 48%—due to lower snowfall and canopy snow loads at these sites, resulting in slightly higher
 339 interception efficiencies for the E10 model. A sensitivity analysis of the canopy snow load
 340 threshold revealed similar model behaviour when using a threshold of 1.6 kg m⁻², based on
 341 observations from Pomeroy & Dion (1996), compared to the 2 kg m⁻² threshold. Differences
 342 between the two models increased for larger canopy snow load thresholds and were slightly
 343 reduced for smaller thresholds.

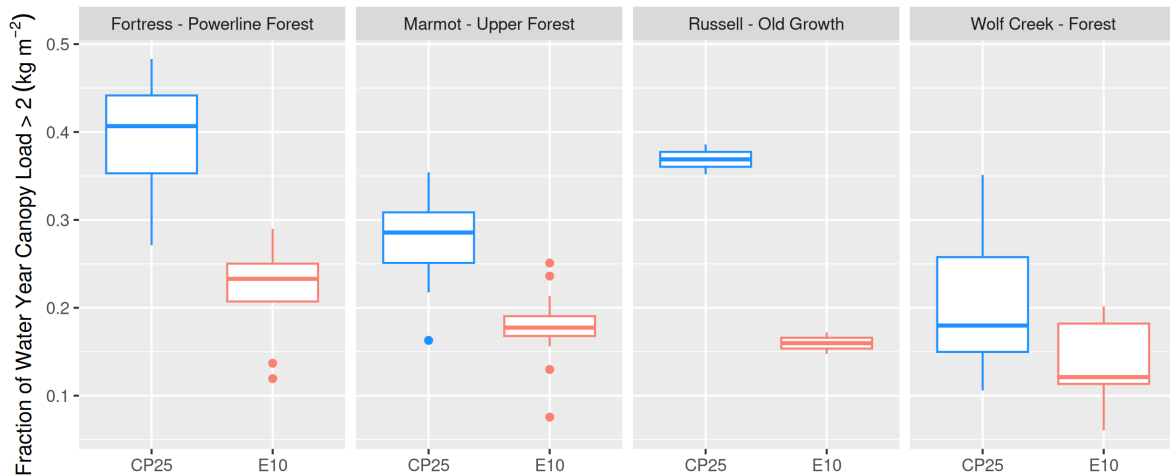


Figure 11: Boxplots showing the annual fraction of time when simulated canopy snow load is greater than 2 kg m⁻² by the CP25 and E10 models.

³⁴⁴ **3.5 Snowfall Partitioning and Disposition**

³⁴⁵ A greater fraction of annual snowfall was sublimated by CP25 compared to E10 for all four sites
³⁴⁶ across all years (Fig. 12). Lower interception efficiency combined with higher average rates
³⁴⁷ of unloading for the E10 model led to more snowfall being partitioned towards the ground
³⁴⁸ compared to the CP25 model (Fig. 12) leading to reduced sublimation of canopy snow and
³⁴⁹ underprediction of canopy SWE (Table 2) and overprediction of subcanopy SWE accumulation
³⁵⁰ (Table 3). The underprediction of subcanopy SWE by the CP25 model at Fortress, Marmot,
³⁵¹ and Wolf Creek (Table 3) may have been due to an overestimate of sublimation and/or canopy
³⁵² snowmelt rates leading to less snowfall being partitioned to the ground as solid snow. The
³⁵³ difference in the annual fraction of snowfall that was sublimated between the CP25 and E10
³⁵⁴ models was most prevalent at Marmot (Fig. 12). Factors that may contribute to this large
³⁵⁵ deviation include the lower unloading rates observed for CP25 at this site (Fig. 12) compared to
³⁵⁶ E10 resulting from the lower wind speed and air temperatures at this site (Fig. 2), reducing the
³⁵⁷ unloading and canopy snowmelt rates, thus increasing the amount of canopy snow subject to
³⁵⁸ sublimation for CP25. At Marmot Creek, the monthly air temperature normals between April
³⁵⁹ and June—when this site receives most of its snowfall (Fig. 2)—are also largely within the E10
³⁶⁰ ice-bulb temperature unloading range (-3°C to 6°C) for initiating unloading due to warming.
³⁶¹ Relatively similar fractions of annual snowfall were sublimated by the two models at Fortress
³⁶² and Wolf Creek (Fig. 12) due to the general agreement in the two sublimation parameterisation
³⁶³ by the two models combined with the similar fraction of snow partitioned towards the ground
³⁶⁴ (Fig. 12). The drip/melt fraction simulated by E10 was near zero for all four sites, while CP25
³⁶⁵ had fractions ranging between 0.1 to 0.38 (Fig. 12). As a result, the E10 model incorrectly
³⁶⁶ partitioned canopy snow ablation entirely as solid snow unloading for melt events and also
³⁶⁷ contributed to the overestimation of subcanopy SWE (Table 3). Process observations of initial
³⁶⁸ interception, unloading, drip, and sublimation were evaluated in Cebulski & Pomeroy (2025b)
³⁶⁹ and Cebulski & Pomeroy (2025c) at Fortress Mountain; however, these observations were not
³⁷⁰ available at the other sites and thus the simulations of snowfall partitioning could not be
³⁷¹ directly evaluated.

³⁷² The results from the new CP25 model show that at Marmot and Wolf Creek, two cold, low-
³⁷³ snowfall sites with calm winds, snowfall was primarily partitioned into sublimation of inter-
³⁷⁴ cepted snow (Fig. 13). At Russell Creek, warm temperatures, high humidities and calm winds
³⁷⁵ resulted in snowfall primarily partitioning into unloading and canopy snow drip. Cold air
³⁷⁶ temperatures and increased wind speeds at Fortress increased the relative contribution of un-
³⁷⁷ loading, compared to melt and sublimation. The difference in throughfall relative to the mean
³⁷⁸ water year snowfall across the four sites results from differences in the calculated snow-leaf
³⁷⁹ contact area used in the initial snow interception calculation, which is a function of the site
³⁸⁰ canopy coverage as well as hydrometeor trajectory zenith angle (departure in degrees from a
³⁸¹ vertical plane) as defined in Cebulski & Pomeroy (2025b).

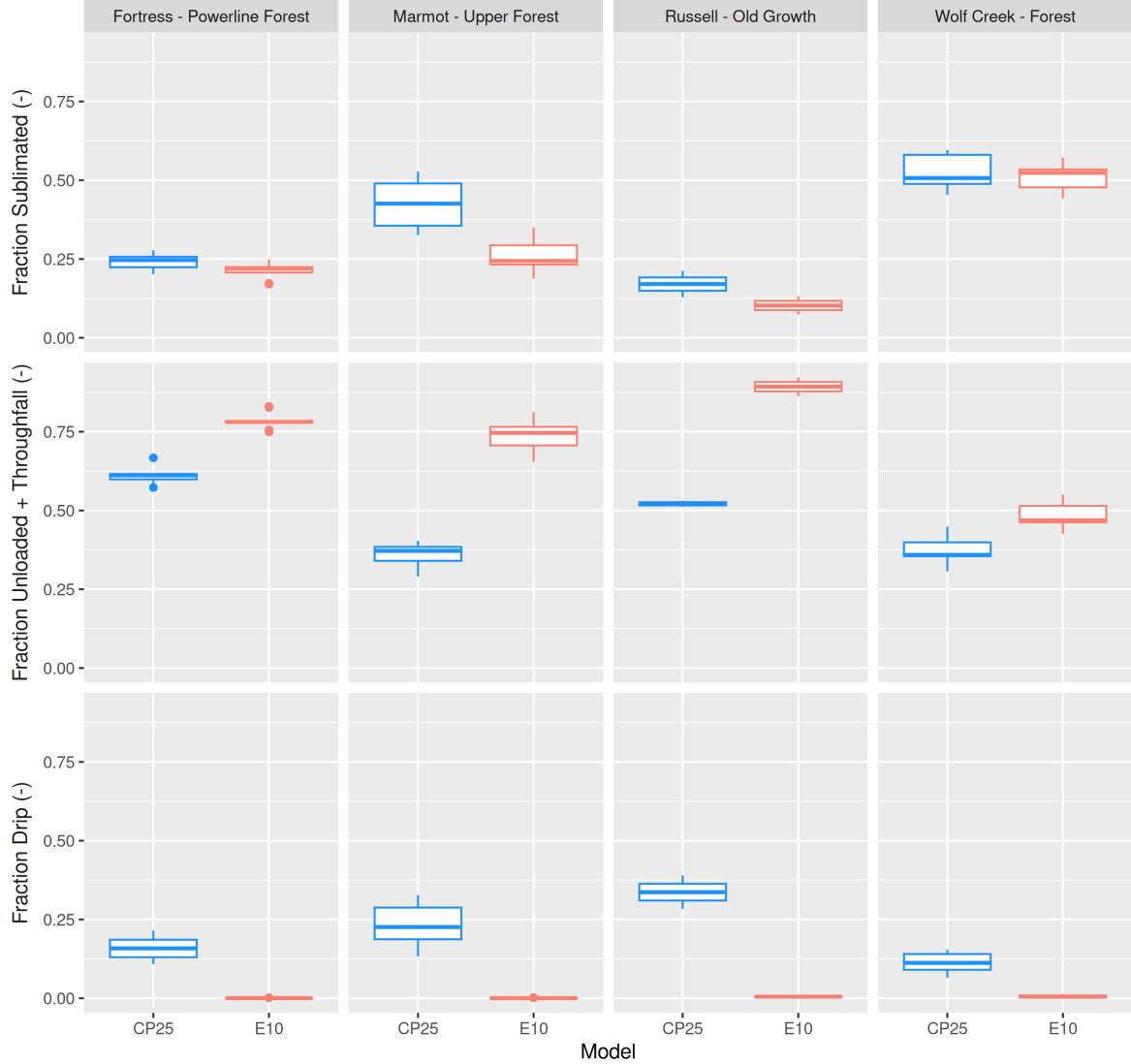


Figure 12: Boxplots showing the distribution of the fraction of total snowfall that was sublimated out of the canopy (top row), reached the subcanopy via unloading and/or throughfall (middle row), and drip from melting intercepted snow (bottom row) at each station for each water year (year ranges are shown in Table 1). Note: the rectangle vertical extent represents the interquartile range (25th to 75th percentile), the horizontal line within each box indicates the median, and the whiskers extend to 1.5 times the interquartile range. Circular points beyond the whiskers represent outliers.

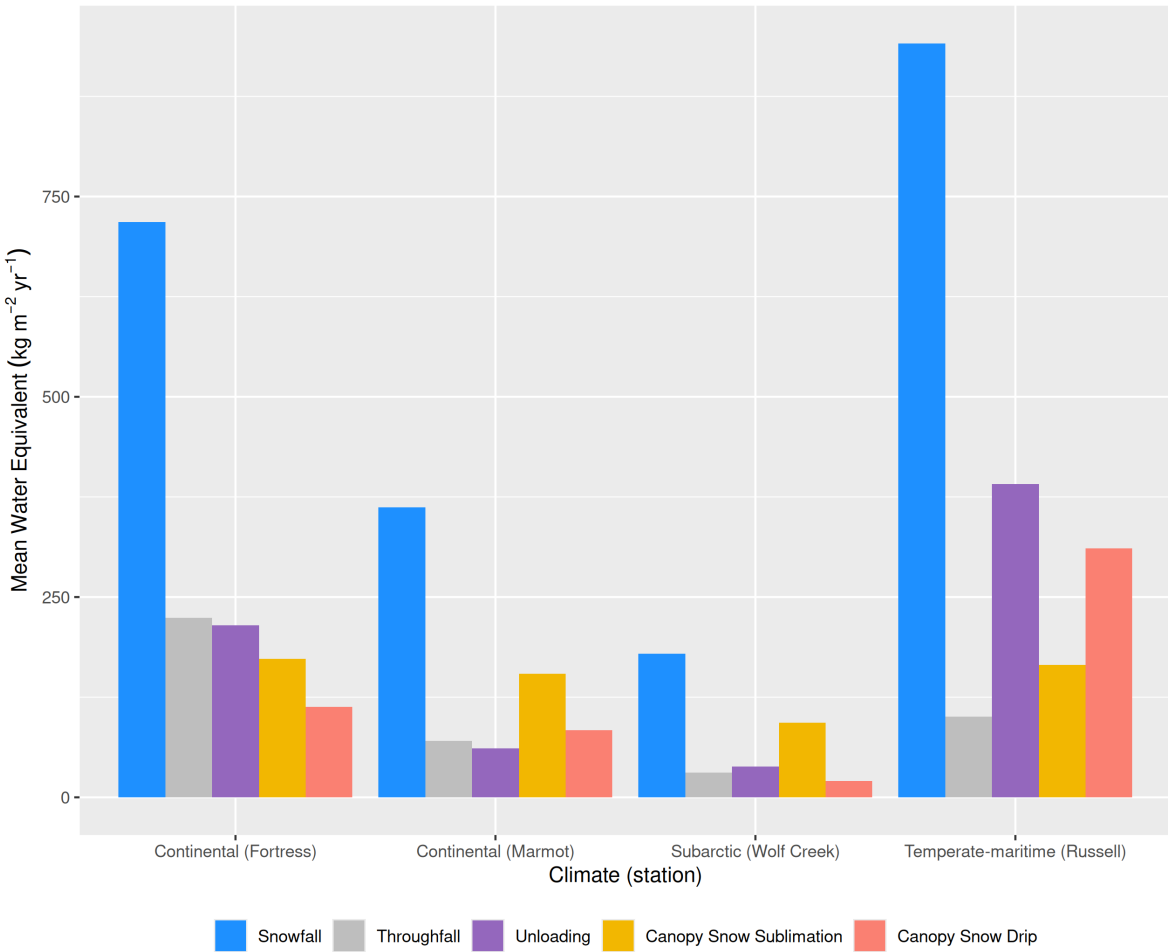


Figure 13: Bar chart of the mean water-year totals of snowfall, throughfall, unloading, canopy snow sublimation, and drip from melting intercepted snow at each station, averaged across all years. The year ranges for each station are given in Table 1.

382 4 Discussion

383 4.1 Model Performance

384 New parameterisations of the canopy snow energy and mass balance—supported by advances
 385 in process understanding (Cebulski & Pomeroy, 2025b, 2025c; Lundquist et al., 2021; Staines
 386 & Pomeroy, 2023)—were evaluated for their ability to simulate SWE stored within and below

the canopy. Inclusion of both dry- and melt-induced unloading is supported by observations (Cebulski & Pomeroy, 2025c; Ellis et al., 2010; Floyd, 2012; Lumbrazo et al., 2022; Roesch et al., 2001), with mechanisms such as bond weakening, lubrication during melt, and wind shear reinforcing their physical basis. An energy balance-based canopy snowmelt routine—recommended by many studies (Andreadis et al., 2009; Cebulski & Pomeroy, 2025c; Essery et al., 2025; Lumbrazo et al., 2022; Lundquist et al., 2021; Storck et al., 2002; Vionnet et al., 2025) also contributed to improved accuracy of simulated canopy and subcanopy SWE. The higher canopy snow loads simulated by the new model are consistent with empirical observations in this study and others (Calder, 1990; Cebulski & Pomeroy, 2025b; Hedstrom & Pomeroy, 1998; Storck et al., 2002; Watanabe & Ozeki, 1964), which demonstrate a linear increase in interception with snowfall and limited evidence of a maximum capacity. Specifically, simulated canopy snow loads reaching close to 50 kg m^{-2} are consistent with observations in coastal environments by Storck et al. (2002) and Floyd (2012). By calculating throughfall as a function of canopy density (Cebulski & Pomeroy, 2025b; Staines & Pomeroy, 2023) and combining this with a comprehensive canopy snow ablation routine (Cebulski & Pomeroy, 2025c; Lundquist et al., 2021), results from Cebulski & Pomeroy (2025b) and Table 2 showed canopy snow loads simulated using the new initial interception parameterisation were more representative of observations. Calculating throughfall as a function of antecedent snow load, as implemented in the E10 model, combined with unloading rates parameterised by ice-bulb temperature and/or canopy snow load, resulted in underestimation of both the amount and duration of snow intercepted in the canopy. While the new model reduced errors in simulated snow load (Fig. 6), canopy snow loads were generally overestimated compared to observations at Marmot Creek for cold snow events and suggests dry-snow unloading rates may be higher in this forest. For mixed rain/snow events canopy snow load was underestimated by the new model and E10 due to underestimates in the liquid water storage capacity and/or overestimates in canopy snow ablation during these events. The liquid water storage capacities for both models were computed using Equation 2 from Cebulski & Pomeroy (2025c), suggesting that the coefficients in this equation may require adjustment for this forest site. Rainfall interception studies have demonstrated that the canopy water storage capacity varies across forest age classes (Pypker

et al., 2005) and species (Xiao & McPherson, 2016). However, further research is needed to understand how liquid water storage capacity differs amongst species and age classes, and how these differences manifest under varying levels of intercepted snow. Moreover, the unloading rates over these warmer events may be lower compared to the coefficients developed at Fortress Mountain in Cebulski & Pomeroy (2025c), potentially due to increases in cohesion and adhesion of snow to the canopy due to increases in liquid water content and/or melt-freeze processes within the canopy. Lumbrazo et al. (2022) also showed that parameters for unloading are site specific and may suggest the initial interception parameters or model process conceptions are as well. However, the large improvement in both the uncalibrated simulation of canopy snow load and intercepted snow duration by the new model provides some evidence of increased transferability across differing forest canopies. Despite some discrepancies in simulating canopy snow load by the new model at Marmot Creek, the new model more closely approximated the duration the canopy was loaded with more than 2 kg m^{-2} of snow—based on the threshold identified by Pomeroy & Dion (1996) to be sufficient to impact above canopy albedo—reducing error compared to an existing model by a factor of four.

The improved representation of canopy snow ablation as demonstrated by Cebulski & Pomeroy (2025c) at Fortress Mountain for individual snowfall events under warm conditions likely contributed to significant reduction in simulated subcanopy SWE errors at the temperate-maritime Russell site. In contrast, the E10 ice-bulb temperature-based melt threshold ($> 6^\circ\text{C}$) was infrequently reached and caused ablation to occur mainly as solid snow unloading rather than drip. Overestimates of canopy snow unloading during both dry-snow and melt-driven conditions by the E10 model led to overpredicted subcanopy SWE, as less intercepted snow was exposed to sublimation or melt (Table 3). Low error in the new model simulated subcanopy SWE at the cold sites (i.e., Fortress, Marmot, and Wolf Creek) suggests that the dry snow unloading parameterisation is transferable across sites and is consistent with observations by Lumbrazo et al. (2022), where a wind-driven unloading parameterisation had good accuracy across differing cold-climate sites. Despite relatively similar mean biases in sub-canopy SWE simulations across the cold-climate sites (Table 3), the new model had reduced

RMSE and higher KGE and NSE values. This resulted from an improved representation of snow interception and canopy snow ablation processes which better captured the variation in snowfall partitioning over years with differing snowfall amounts and meteorology. Both the new model and E10 model performed worst at the temperate-maritime Russell site—although the new model showed large improvements over E10—where melt/drip and melt-induced unloading processes dominated. Remaining error at Russell may reflect unrepresented processes, such as ice accretion from canopy snow melt-freeze cycles and rime-ice deposition as observed in other maritime forests (Lumbrazo et al., 2022), which can increase canopy loads, lower unloading rates, and favour partitioning to liquid water. Additional uncertainties stem from simplifications in the canopy energy balance (e.g., radiation transmittance, longwave emission, and turbulent fluxes), as well as parameterisations of interception and unloading (Cebulski & Pomeroy, 2025b, 2025c). These issues are likely amplified at Russell, where frequent air temperatures near the melting point cause large changes in enthalpy which increase phase change sensitivity to energy balance formulations, compared to the colder sites with more stable enthalpy conditions. Some errors in subcanopy SWE simulations are also attributed to limitations in the subcanopy snowpack energy and mass balance routine (i.e., Snobal). For instance, a minimum accumulation threshold caused discrepancies in subcanopy SWE simulations at Wolf Creek.

The hydrometeor fall velocity and wind shear stress used in the initial interception and canopy snow unloading parameterisations, respectively, were estimated using simplified approximations that introduced error into the new model’s results at all four sites. For instance, a fixed hydrometeor fall velocity was used at all four sites based on empirical observations from Cebulski & Pomeroy (2025b) and Isyumov (1971). This approximation increases uncertainty in the initial interception calculation due to the associated sensitivity of wind speed and hydrometeor fall velocity with snow-leaf contact area. Furthermore, midcanopy shear stress was approximated using an empirical relationship with midcanopy wind speed developed in Cebulski & Pomeroy (2025c). The use of more physically based formulations that account for variations in shear stress resulting from differences in air density and/or within-canopy wind flow (Stull,

472 2017) could further improve estimates of shear stress and, consequently, unloading.

473 The new model simulated much longer periods of canopy load greater than 2 kg m^{-2} and im-
474 proved accuracy at Marmot Creek compared to an existing approach (Table 2). Sensitivity
475 to the canopy snow load threshold was observed, with greater intermodel discrepancies for
476 larger threshold values and slightly smaller differences for lower thresholds. Greater model
477 differences were observed for the larger thresholds as the new model predicted much larger
478 canopy snow loads across all sites and years (Fig. 10). This improved simulation of canopy
479 snow load has implications for the representation of above-canopy albedo in land surface mod-
480 els which have previously shown poor performance with existing canopy snow ablation models
481 (Thackeray et al., 2014; Wang et al., 2016). Moreover, E10's performance in simulating sub-
482 canopy SWE varied substantially between years; it overestimated SWE over most years, but
483 underestimated SWE in low-snowfall years when reduced unloading rates allowed more subli-
484 mation (e.g., Marmot in 2019; Fig. 7). These results show that recent improvements in process
485 parameterisations—particularly the treatment of canopy load, ablation, and unloading—yield
486 measurable improvements in simulating canopy and subcanopy SWE across diverse climates
487 and forest types.

488 Several existing models (Clark et al., 2015; Elshamy et al., 2025; Essery et al., 2025; Vion-
489 net et al., 2025) employ parameterisations similar to the E10 model (based on Hedstrom &
490 Pomeroy (1998) and Ellis et al. (2010)); however, the results presented here indicate improved
491 performance in simulating SWE below and within the canopy when using the newer parame-
492 terisations developed by Cebulski & Pomeroy (2025b) and Cebulski & Pomeroy (2025c). The
493 new model represents intercepted snow using a single-layer mass and energy balance, consis-
494 tent with approaches adopted in other recent studies (e.g., Vionnet et al., 2025). Although
495 multi-layer representations of intercepted snow have been proposed (Clark et al., 2015; Essery
496 et al., 2025), such an approach was not implemented here due to uncertainties in estimating
497 model forcing variables at multiple heights within the canopy. Nevertheless, the development
498 and evaluation of multi-layer canopy snow schemes remains a promising direction for future
499 research, particularly where adequate observational constraints are available.

500 **4.2 Influence of Climate on Snowfall Partitioning and Disposition**

501 Although Russell and Fortress received similar amounts of snowfall (Fig. 3), subcanopy accu-
502 mulation was 50% lower at Russell due to greater canopy snowmelt: ~40% of annual snowfall
503 melted and 20% sublimated in the canopy, compared to ~35% combined melt and sublimation
504 of intercepted snow at Fortress. The low cold content of the maritime snowpack at Russell
505 limited refreezing of canopy snow meltwater, and relatively warm air temperatures (Fig. 2) pro-
506 moted melt of the subcanopy snowpack throughout the season, reducing subcanopy snowpack
507 accumulation (Fig. 7). Consequently, the prevalence of snowmelt both in the canopy and on
508 the ground at Russell led to the lowest fraction of seasonal snowfall stored as subcanopy snow
509 accumulation at peak SWE (Fig. 4). Canopy snow sublimation was also lowest at Russell, as
510 most ablation occurred via melt and solid snow unloading (Fig. 12, Fig. 13). Frequent mid-
511 winter canopy snowmelt also provided a steady year-round input of drip to the subcanopy,
512 which recharges soil moisture and groundwater, and promotes runoff generation (Barnhart
513 et al., 2016; Groff & Pomeroy, 2025; Hayashi, 2020). At Fortress, colder conditions, higher
514 seasonal snowfall, and greater wind exposure increased unloading rates and limited canopy
515 snow sublimation (Fig. 12, Fig. 13). Combined with low canopy snow drip (Fig. 13), these
516 processes at Fortress yielded the highest subcanopy accumulation (0.6) across all four sites
517 (Fig. 4). Marmot and Wolf Creek experienced cooler, drier conditions with calm winds and
518 lower seasonal snowfall, leading to reduced unloading and increased the fraction and amount
519 of snowfall that was sublimated from the canopy (Fig. 12, Fig. 13). This, coupled with canopy
520 snowmelt playing a minor role in partitioning intercepted snow meant that only ~0.4 of snow-
521 fall accumulated as subcanopy snowpack at peak SWE (Fig. 4). Simulated sublimation at
522 Marmot and Wolf Creek (~50% of seasonal snowfall; Fig. 12) exceeded the upper range of
523 global estimates (25–45%) reported by Essery et al. (2003) but is consistent with observations
524 by Pomeroy & Gray (1995), Pomeroy et al. (1998), and Ellis et al. (2010).

525 These results also extend earlier discussions by Pomeroy & Gray (1995) on the fraction of
526 seasonal snowfall stored in forests, by demonstrating how the partitioning and disposition

of intercepted snow varies across differing climates and forests (Fig. 13). At Russell Creek, a temperate forest, snowfall was predominantly partitioned into unloading and canopy snow drip, with minimal sublimation. At Marmot and Wolf Creek two cold-regions forests, characterised by low seasonal snowfall and calm winds, snowfall was primarily returned to the atmosphere via sublimation of intercepted snow. Fortress, a cold, wind-exposed forest with higher snowfall, was dominated by unloading. The agreement in the new model and E10 in partitioning snowfall between sublimation and unloading at Fortress and Wolf Creek arises because the E10 routine unloads a similar fraction of annual snowfall as the new model despite having different parameterisations for unloading and sublimation. For the two sublimation schemes, E10 omits longwave radiation from the canopy snow sublimation energy balance (Pomeroy et al., 1998), while parameterisation used in the new model includes longwave radiation (Essery et al., 2003). This consistency between the two sublimation parameterisations was also observed by Cebulski & Pomeroy (2025c) during several sublimation-dominated ablation events.

4.3 Influence of Tree Species on Snowfall Partitioning

The species of needleleaf forest overlying each site also influenced subcanopy SWE accumulation. However, limited research has been conducted on how branch elasticity, needle composition, and crown structure between differing species and ages affect the interception and ablation of snow. The Marmot and Wolf Creek sites, both primarily composed of spruce trees (Table 1) and exposed to similarly cool climates (Fig. 2), showed comparable fractions of snowfall stored in the subcanopy (Fig. 11) and similar canopy melt and sublimation losses (Fig. 12). In contrast, Fortress and Russell were both primarily fir-dominated forests, yet diverged strongly due to climate differences (Fig. 2) and vegetation structure. Even though Russell had approximately 20% more canopy cover than Fortress, it accumulated only about half as much snowfall beneath the canopy. Tree size is a likely factor, large 50 m tall fir trees at Russell can intercept far more snow than the smaller 10 m fir trees at Fortress. Coupled with low wind speeds, this increased exposure of intercepted snow to canopy energy fluxes that favoured melt and drip at Russell Creek. The larger, more supportive branches combined

with the differing climatic regime and potential for ice-deposition may also have slowed unloading, contributing to the new model's overestimate of subcanopy SWE at Russell. These results support earlier theory posed by Satterlund & Haupt (1970) that vegetation structure, density, and climate exert stronger control on forest-snow partitioning than tree species alone. Moreover, Schmidt & Pomeroy (1990) showed that branch temperature rather than species type had the greatest influence on the modulus of elasticity of needleleaf branches and their snow holding capacity. However, other forest types, such as broadleaf deciduous (Huerta et al., 2019), cedar or hemlock stands, or younger trees, with less supportive leaves and branches, may have a stronger influence on canopy-snow processes than the relatively subtle species differences observed amongst needleleaf sites in this study.

5 Conclusions

Recent advances in canopy snow energy and mass balance parameterisations were shown to reduce errors in simulated SWE, both within and below the canopy, across forests spanning a range of climates and canopy structures. The new model also provided a more robust diagnosis of the processes that govern how intercepted snowfall is partitioned between sublimation to the atmosphere, storage in the canopy, drip, and unloading to the forest floor. Building on recent developments, the new approach calculates initial snow interception as a function of canopy density and hydrometeor trajectory angle. Canopy snow ablation is represented by melt- and wind-driven unloading, energy balance-based melt, and sublimation processes that vary with canopy snow load. The new parameterisations improved simulations of the quantity and duration that snow was intercepted in the canopy compared to an existing approach. Simulation of subcanopy SWE improved across all four sites and is attributed to more accurately representing the canopy snow energy and mass balance in the new model. This was most apparent in a temperate-maritime environment, where errors in subcanopy SWE were a factor of four lower—attributed to a more accurate representation of initial interception, canopy snowmelt, and unloading. These results highlight the robustness of physically based parameterisations

580 over a wide range of climatic conditions, which is particularly important given that continued
581 warming may reduce the applicability of empirically derived routines.

582 Process diagnosis conducted with the new snow interception and canopy snow ablation pa-
583 rameterisations highlighted the role of needleleaf canopies in partitioning intercepted snowfall.
584 The greatest influence was observed in the temperate-maritime forest, where increased energy
585 fluxes to intercepted snow caused nearly half of seasonal snowfall to melt within the canopy,
586 producing the lowest subcanopy SWE fraction of snowfall and a steady contribution of melt-
587 water throughout the winter. Despite the large influence of snowfall partitioning by vegetation
588 on the subcanopy snowpack, sublimation losses were relatively small (~20% of seasonal snow-
589 fall). At two cold continental sites with lower annual snowfall, reduced unloading led to a
590 larger proportion of intercepted snow to be retained in the canopy over longer durations and
591 returned to the atmosphere via sublimation (~40%). In contrast, the cold wind-exposed site
592 with higher snowfall exhibited greater unloading and shorter canopy residence times, which
593 limited sublimation losses relative to the other cold sites. Overall, the partitioning and dispo-
594 sition of intercepted snow was observed to strongly vary across climates: temperate-maritime
595 forests were dominated by canopy snow drip, cold, wind-exposed forests by unloading, and
596 cold, forests with calm winds by sublimation. Across all sites, climate and canopy density ex-
597 ereted stronger controls on seasonal snowfall partitioning than species-level differences between
598 fir-, spruce-, and pine-dominated forests.

599 Although the new model simulated canopy and subcanopy SWE well, uncertainties remain in
600 partitioning of snowfall between sublimation losses and liquid water inputs to the forest floor,
601 as direct flux measurements have only been validated at one site in a previous study. Mea-
602 surements of snow interception, unloading, drip, and sublimation are rarely made at hydrom-
603 eteorological stations but would provide important data to evaluate and refine process-level
604 representations across differing environments. Further research is also needed to determine
605 differences in the unloading relationships across a broad range in climate and forest types. For
606 instance, unloading can be strongly affected by branch elasticity variations with temperature,
607 tree age, and/or tree species. Differing cohesion and adhesion in humid climates may influ-

ence how snow is retained or shed from canopies compared to the coefficients implemented here which were developed in a continental climate. Moreover, all four study sites consisted primarily of mature needleleaf forest canopies, and the transferability of these results to more juvenile stands or forests with greater species diversity remains an open area of research. Improved process-level measurements, combined with continued model development, will help to identify these uncertainties and support the transferability of canopy snow models across the wide range of conditions found in snowy forests across the globe.

6 Acknowledgements

We acknowledge financial support from the University of Saskatchewan Dean's Scholarship, the Natural Sciences and Engineering Research Council of Canada's Discovery Grants, the Canada First Research Excellence Fund's Global Water Futures Programme, Environment and Climate Change Canada, Alberta Innovates Water Innovation Program, the Canada Foundation for Innovation's Global Water Futures Observatories facility, and the Canada Research Chairs Programme. We thank Hannah Koslowsky, Kieran Lehan, Lindsey Langs, James MacDonald, Michael Solohub, Jacob Staines, Greg Galloway, Sean Carey, Rosy Tutton, David Barrett, and Tyler De Jong for their help with data collection and Tom Brown and Logan Fang for support of the CRHM platform.

7 Data and Software Availability Statement

The Cold Regions Hydrological Model Platform (CRHM) source code used in this study is preserved at <https://doi.org/10.5281/zenodo.17981431> (Pomeroy et al., 2025), available under the GPL-3.0 licence, and developed openly at <https://github.com/srlabUsask/crhmcode>. Model forcing data, model outputs, validation data, processed data, and scripts to run the processing are available at <https://doi.org/10.5281/zenodo.17409551> with GPL-3.0 licence access conditions.

632 **References**

- 633 Andreadis, K. M., Storck, P., & Lettenmaier, D. P. (2009). Modeling snow accumulation
634 and ablation processes in forested environments. *Water Resources Research*, 45(5), 1–33.
635 <https://doi.org/10.1029/2008WR007042>
- 636 Annandale, J., Jovanovic, N., Benadé, N., & Allen, R. (2002). Software for missing data
637 error analysis of Penman-Monteith reference evapotranspiration. *Irrigation Science*, 21(2),
638 57–67. <https://doi.org/10.1007/s002710100047>
- 639 Barnhart, T. B., Molotch, N. P., Livneh, B., Harpold, A. A., Knowles, J. F., & Schneider, D.
640 (2016). Snowmelt rate dictates streamflow. *Geophysical Research Letters*, 43(15), 8006–
641 8016. <https://doi.org/10.1002/2016gl069690>
- 642 Brutsaert, W. (1982). *Evaporation into the Atmosphere: Theory, History, and Applications*.
643 Dordrecht, Holland: Reidel.
- 644 Calder, I. R. (1990). *Evaporation in the Uplands* (p. 148). Wiley.
- 645 Canada Centre for Remote Sensing, Canada Centre for Mapping and Earth Observation &
646 Natural Resources Canada. (2020). *Land Cover of North America at 30 meters* [Raster
647 Digital Data].
- 648 Cebulski, A. C., & Pomeroy, J. W. (2025a). Theoretical underpinnings of snow interception
649 and canopy snow ablation parameterisations. *WIREs Water*, 12, e70010. <https://doi.org/>
650 [10.1002/wat2.70010](https://doi.org/10.1002/wat2.70010)
- 651 Cebulski, A. C., & Pomeroy, J. W. (2025b). Snow interception relationships with meteorology
652 and canopy density. *Hydrological Processes*, 39(4), e70135. <https://doi.org/10.1002/hyp.>
653 [70135](https://doi.org/10.1002/hyp.70135)
- 654 Cebulski, A. C., & Pomeroy, J. W. (2025c). Processes governing the ablation of intercepted
655 snow. *Water Resources Research*, *in review*.
- 656 Clark, M. P., Nijssen, B., Lundquist, J. D., Kavetski, D., Rupp, D. E., Woods, R. A., Freer,
657 J. E., Gutmann, E. D., Wood, A. W., Brekke, L. D., Arnold, J. R., Gochis, D. J., &
658 Rasmussen, R. M. (2015). A unified approach for process-based hydrologic modeling: 1.
659 Modeling concept. *Water Resources Research*, 51(4), 2498–2514. <https://doi.org/10.1002/>

- 660 2015WR017198
- 661 Clark, M. P., Vogel, R. M., Lamontagne, J. R., Mizukami, N., Knoben, W. J. M., Tang, G.,
662 Gharari, S., Freer, J. E., Whitfield, P. H., Shook, K. R., & Papalexiou, S. M. (2021). The
663 abuse of popular performance metrics in hydrologic modeling. *Water Resources Research*,
664 57(9), 1–16. <https://doi.org/10.1029/2020WR029001>
- 665 Deschamps-Berger, C., López-Moreno, J. I., Gascoin, S., Mazzotti, G., & Boone, A. (2025).
666 Where snow and forest meet: A global atlas. *Geophysical Research Letters*, 52(10),
667 e2024GL113684. <https://doi.org/10.1029/2024GL113684>
- 668 Ellis, C. R., Pomeroy, J. W., Brown, T., & MacDonald, J. (2010). Simulation of snow accumu-
669 lation and melt in needleleaf forest environments. *Hydrology and Earth System Sciences*,
670 14(6), 925–940. <https://doi.org/10.5194/hess-14-925-2010>
- 671 Elshamy, M. E., Pomeroy, J. W., Pietroniro, A., Wheater, H., & Abdelhamed, M. (2025).
672 The Impact of Climate and Land Cover Change on the Cryosphere and Hydrology of
673 the Mackenzie River Basin, Canada. *Water Resources Research*, 61(12), e2024WR039276.
674 <https://doi.org/10.1029/2024WR039276>
- 675 Essery, R., Mazzotti, G., Barr, S., Jonas, T., Quaife, T., & Rutter, N. (2025). A Flexible Snow
676 Model (FSM 2.1.0) including a forest canopy. *EGUsphere*, 1–37. <https://doi.org/10.5194/egusphere-2024-2546>
- 677 Essery, R., Pomeroy, J. W., Parviainen, J., & Storck, P. (2003). Sublimation of snow from
678 coniferous forests in a climate model. *Journal of Climate*, 16(11), 1855–1864. [https://doi.org/10.1175/1520-0442\(2003\)016%3C1855:SOSFCF%3E2.0.CO;2](https://doi.org/10.1175/1520-0442(2003)016%3C1855:SOSFCF%3E2.0.CO;2)
- 679 Fang, X., Pomeroy, J. W., Debeer, C. M., Harder, P., & Siemens, E. (2019). Hydrometeo-
680 rological data from marmot creek research basin, canadian rockies. *Earth System Science
681 Data*, 11(2), 455–471. <https://doi.org/10.5194/essd-11-455-2019>
- 682 Floyd, W. C. (2012). *Snowmelt Energy Flux Recovery During Rain-on-Snow in Regenerating
683 Forests* (p. 180) [PhD thesis, University of British Columbia]. <https://doi.org/10.14288/1.0073024>
- 684 Garnier, B. J., & Ohmura, A. (1970). The evaluation of surface variations in solar radiation
685 income. *Solar Energy*, 13(1), 21–34. [https://doi.org/10.1016/0038-092X\(70\)90004-6](https://doi.org/10.1016/0038-092X(70)90004-6)

- 689 Gelfan, A. N., Pomeroy, J. W., & Kuchment, L. S. (2004). Modeling forest cover influences on
690 snow accumulation, sublimation, and melt. *Journal of Hydrometeorology*, 5(5), 785–803.
691 [https://doi.org/10.1175/1525-7541\(2004\)005%3C0785:MFCIOS%3E2.0.CO;2](https://doi.org/10.1175/1525-7541(2004)005%3C0785:MFCIOS%3E2.0.CO;2)
- 692 Groff, T., & Pomeroy, J. W. (2025). Snowmelt Infiltration and Runoff From Seasonally Frozen
693 Hillslopes in a High Mountain Basin. *Hydrological Processes*, 39(1), e70048. <https://doi.org/10.1002/hyp.70048>
- 694 Gupta, H. V., Kling, H., Yilmaz, K. K., & Martinez, G. F. (2009). Decomposition of the
695 mean squared error and NSE performance criteria: Implications for improving hydrological
696 modelling. *Journal of Hydrology*, 377(1-2), 80–91. <https://doi.org/10.1016/j.jhydrol.2009.08.003>
- 697 Harder, P., & Pomeroy, J. W. (2013). Estimating precipitation phase using a psychrometric
698 energy balance method. *Hydrological Processes*, 27(13), 1901–1914. <https://doi.org/10.1002/hyp.9799>
- 700 Hayashi, M. (2020). Alpine hydrogeology: The critical role of groundwater in sourcing the
701 headwaters of the world. *Groundwater*, 58(4), 498–510. <https://doi.org/10.1111/gwat.12965>
- 702 Hedstrom, N. R., & Pomeroy, J. W. (1998). Measurements and modelling of snow interception
703 in the boreal forest. *Hydrological Processes*, 12(10-11), 1611–1625.
- 704 Huerta, M. L., Molotch, N. P., & McPhee, J. (2019). Snowfall interception in a deciduous
705 Nothofagus forest and implications for spatial snowpack distribution. *Hydrological Pro-
706 cesses*, 33(13), 1818–1834.
- 707 Immerzeel, W. W., Lutz, A. F., Andrade, M., Bahl, A., Biemans, H., Bolch, T., Hyde, S.,
708 Brumby, S., Davies, B. J., Elmore, A. C., Emmer, A., Feng, M., Fernández, A., Haritashya,
709 U., Kargel, J. S., Koppes, M., Kraaijenbrink, P. D. A., Kulkarni, A. V., Mayewski, P. A., ...
710 Baillie, J. E. M. (2020). Importance and vulnerability of the world's water towers. *Nature*,
711 577(7790), 364–369. <https://doi.org/10.1038/s41586-019-1822-y>
- 712 Isyumov, N. (1971). *An Approach to the Prediction of Snow Loads* [PhD thesis]. The University
713 of Western Ontario (Canada).
- 714 Kim, E., Gatebe, C., Hall, D., Newlin, J., Misakonis, A., Elder, K., Marshall, H. P., Hiem-

- 718 stra, C., Brucker, L., De Marco, E., Crawford, C., Kang, D. H., & Entin, J. (2017).
719 NASA's snowex campaign: Observing seasonal snow in a forested environment. *2017*
720 *IEEE International Geoscience and Remote Sensing Symposium (IGARSS)*, 1388–1390.
721 <https://doi.org/10.1109/IGARSS.2017.8127222>
- 722 Krinner, G., Derksen, C., Essery, R., Flanner, M., Hagemann, S., Clark, M. P., Hall, A., Rott,
723 H., Brutel-Vuilmet, C., Kim, H., Ménard, C. B., Mudryk, L., Thackeray, C., Wang, L.,
724 Arduini, G., Balsamo, G., Bartlett, P., Boike, J., Boone, A., ... Zhu, D. (2018). ESM-
725 SnowMIP: Assessing snow models and quantifying snow-related climate feedbacks. *Geosci-
726 entific Model Development*, 11(12), 5027–5049. <https://doi.org/10.5194/gmd-11-5027-2018>
- 727 Langs, L. E., Petrone, R. M., & Pomeroy, J. W. (2020). A $\delta^{18}\text{O}$ and $\delta^2\text{H}$ stable water
728 isotope analysis of subalpine forest water sources under seasonal and hydrological stress
729 in the Canadian Rocky Mountains. *Hydrological Processes*, 34(26), 5642–5658. <https://doi.org/10.1002/hyp.13986>
- 730 Leach, J. A., & Moore, R. D. (2014). Winter stream temperature in the rain-on-snow zone of
731 the Pacific Northwest: Influences of hillslope runoff and transient snow cover. *Hydrology
732 and Earth System Sciences*, 18(2), 819–838. <https://doi.org/10.5194/hess-18-819-2014>
- 733 López-Moreno, J. I., Zabalza, J., Vicente-Serrano, S. M., Revuelto, J., Gilaberte, M., Azorin-
734 Molina, C., Morán-Tejeda, E., García-Ruiz, J. M., & Tague, C. (2014). Impact of climate
735 and land use change on water availability and reservoir management: Scenarios in the
736 Upper Aragón River, Spanish Pyrenees. *Science of The Total Environment*, 493, 1222–
737 1231. <https://doi.org/10.1016/j.scitotenv.2013.09.031>
- 738 Lumbrazo, C., Bennett, A., Currier, W. R., Nijssen, B., & Lundquist, J. (2022). Evalu-
739 uating multiple canopy-snow unloading parameterizations in SUMMA with time-lapse
740 photography characterized by citizen scientists. *Water Resources Research*, 58(6), 1–22.
741 <https://doi.org/10.1029/2021WR030852>
- 742 Lundquist, J. D., Dickerson-Lange, S., Gutmann, E., Jonas, T., Lumbrazo, C., & Reynolds, D.
743 (2021). Snow interception modelling: Isolated observations have led to many land surface
744 models lacking appropriate temperature sensitivities. *Hydrological Processes*, 35(7), 1–20.
745 <https://doi.org/10.1002/hyp.14274>

- 747 MacDonald, J. P. (2010). *Unloading of Intercepted Snow in Conifer Forests* (p. 93) [Msc
748 Thesis]. University of Saskatchewan.
- 749 Marks, D., & Dozier, J. (1992). Climate and energy exchange at the snow surface in the Alpine
750 Region of the Sierra Nevada: 2. Snow cover energy balance. *Water Resources Research*,
751 28(11), 3043–3054. <https://doi.org/10.1029/92WR01483>
- 752 Marks, D., Kimball, J., Tingey, D., & Link, T. (1998). The sensitivity of snowmelt processes
753 to climate conditions and forest cover during rain-on-snow: A case study of the 1996 Pacific
754 Northwest flood. *Hydrological Processes*, 12(10-11), 1569–1587. [https://doi.org/10.1002/\(SICI\)1099-1085\(199808/09\)12:10/11%3C1569::AID-HYP682%3E3.0.CO;2-L](https://doi.org/10.1002/(SICI)1099-1085(199808/09)12:10/11%3C1569::AID-HYP682%3E3.0.CO;2-L)
- 756 Mazzotti, G., Webster, C., Essery, R., & Jonas, T. (2021). Increasing the physical rep-
757 resentation of forest-snow processes in coarse-resolution models: Lessons learned from
758 upscaling hyper-resolution simulations. *Water Resources Research*, 57(5), 1–21. <https://doi.org/10.1029/2020WR029064>
- 760 Nash, J. E., & Sutcliffe, J. V. (1970). River flow forecasting through conceptual models part
761 I — A discussion of principles. *Journal of Hydrology*, 10(3), 282–290. [https://doi.org/10.1016/0022-1694\(70\)90255-6](https://doi.org/10.1016/0022-1694(70)90255-6)
- 763 Pomeroy, J. W., Brown, T., Fang, X., Shook, K. R., Pradhananga, D., Armstrong, R., Harder,
764 P., Marsh, C., Costa, D., Krogh, S. A., Aubry-Wake, C., Annand, H., Lawford, P., He,
765 Z., Kompanizare, M., & Moreno, J. I. L. (2022). The cold regions hydrological modelling
766 platform for hydrological diagnosis and prediction based on process understanding. *Journal
767 of Hydrology*, 615(128711), 1–25. <https://doi.org/10.1016/j.jhydrol.2022.128711>
- 768 Pomeroy, J. W., Brown, T., Fang, X., Shook, K. R., Pradhananga, D., Armstrong, R., Harder,
769 P., Marsh, C., Costa, D., Krogh, S. A., Aubry-Wake, C., Annand, H., Lawford, P., He, Z.,
770 Kompanizare, M., Moreno, J. I. L., & Cebulski, A. C. (2025). *The cold regions hydrological
771 modelling platform [software]*. Zenodo. <https://doi.org/10.5281/zenodo.17981431>
- 772 Pomeroy, J. W., & Dion, K. (1996). Winter radiation extinction and reflection in a boreal
773 pine canopy: Measurements and modelling. *Hydrological Processes*, 10(12), 1591–1608.
774 [https://doi.org/10.1002/\(sici\)1099-1085\(199612\)10:12%3C1591::aid-hyp503%3E3.0.co;2-8](https://doi.org/10.1002/(sici)1099-1085(199612)10:12%3C1591::aid-hyp503%3E3.0.co;2-8)
- 775 Pomeroy, J. W., Essery, R. L. H., & Helgason, W. D. (2016). Aerodynamic and radiative

- 776 controls on the snow surface temperature. *Journal of Hydrometeorology*, 17(8), 2175–2189.
- 777 <https://doi.org/10.1175/JHM-D-15-0226.1>
- 778 Pomeroy, J. W., & Gray, D. M. (1995). *Snowcover Accumulation, Relocation and Management*
779 (NHRI Science Report No. 7, p. 144). National Hydrology Research Institute, Environment
780 Canada, Saskatoon, Canada.
- 781 Pomeroy, J. W., Marks, D., Link, T., Ellis, C. R., Hardy, J., Rowlands, A., & Granger, R.
782 (2009). The impact of coniferous forest temperature on incoming longwave radiation to
783 melting snow. *Hydrological Processes*, 23, 2513–2525. <https://doi.org/10.1002/hyp.7325>
- 784 Pomeroy, J. W., Parviainen, J., Hedstrom, N., & Gray, D. M. (1998). Coupled modelling of
785 forest snow interception and sublimation. *Hydrological Processes*, 12(15), 2317–2337. [https://doi.org/10.1002/\(SICI\)1099-1085\(199812\)12:15%3C2317::AID-HYP799%3E3.0.CO;2-X](https://doi.org/10.1002/(SICI)1099-1085(199812)12:15%3C2317::AID-HYP799%3E3.0.CO;2-X)
- 787 Pomeroy, J. W., Rowlands, A., Hardy, J., Link, T., Marks, D., Essery, R., Sicart, J. E., & Ellis,
788 C. R. (2008). Spatial variability of shortwave irradiance for snowmelt in forests. *Journal
789 of Hydrometeorology*, 9(6), 1482–1490.
- 790 Pomeroy, J. W., & Schmidt, R. A. (1993). The use of fractal geometry in modelling intercepted
791 snow accumulation and sublimation. *Eastern Snow Conference*, 50, 231–239.
- 792 Pypker, T. G., Bond, B. J., Link, T. E., Marks, D., & Unsworth, M. H. (2005). The importance
793 of canopy structure in controlling the interception loss of rainfall : Examples from a young
794 and an old-growth Douglas-fir forest. *Agricultural and Forest Meteorology*, 130, 113–129.
795 <https://doi.org/10.1016/j.agrformet.2005.03.003>
- 796 Rasouli, K., Pomeroy, J. W., Janowicz, J. R., Williams, T. J., & Carey, S. K. (2019). A
797 long-term hydrometeorological dataset (1993–2014) of a northern mountain basin: Wolf
798 creek research basin, yukon territory, canada. *Earth System Science Data*, 11(1), 89–100.
799 <https://doi.org/10.5194/essd-11-89-2019>
- 800 Roesch, A., Wild, M., Gilgen, H., & Ohmura, A. (2001). A new snow cover fraction parame-
801 terization for the ECHAM4 GCM. *Climate Dynamics*, 17(12), 933–946. <https://doi.org/10.1007/s003820100153>
- 803 Rojas-Heredia, F., Revuelto, J., Deschamps-Berger, C., Alonso-González, E., Domínguez-
804 Aguilar, P., García, J., Pérez-Cabello, F., & López-Moreno, J. I. (2024). Snow depth

- 805 distribution in canopy gaps in central pyrenees. *Hydrological Processes*, 38(11), e15322.
806 <https://doi.org/10.1002/hyp.15322>
- 807 Rutter, N., Essery, R., Pomeroy, J. W., Altimir, N., Andreadis, K. M., Baker, I., Barr, A.,
808 Bartlett, P., Boone, A., Deng, H., Douville, H., Dutra, E., Elder, K., Ellis, C. R., Feng, X.,
809 Gelfan, A., Goodbody, A., Gusev, Y., Gustafsson, D., ... Yamazaki, T. (2009). Evaluation of
810 forest snow processes models (SnowMIP2). *Journal of Geophysical Research: Atmospheres*,
811 114(D6), 10–18. <https://doi.org/10.1029/2008JD011063>
- 812 Sanmiguel-Vallelado, A., Morán-Tejeda, E., Alonso-González, E., & López-Moreno, J. I. (2017).
813 Effect of snow on mountain river regimes: An example from the Pyrenees. *Frontiers of*
814 *Earth Science*, 11(3), 515–530. <https://doi.org/10.1007/s11707-016-0630-z>
- 815 Satterlund, D. R., & Haupt, H. F. (1970). The disposition of snow caught by conifer crowns.
816 *Water Resources Research*, 6(2), 649–652. <https://doi.org/10.1029/WR006i002p00649>
- 817 Schmidt, R. A., & Pomeroy, J. W. (1990). Bending of a conifer branch at subfreezing temper-
818 atures: Implications for snow interception. *Canadian Journal of Forest Research*, 20(8),
819 1251–1253. <https://doi.org/10.1139/x90-165>
- 820 Shook, K., & Pomeroy, J. (2011). Synthesis of incoming shortwave radiation for hydrological
821 simulation. *Hydrology Research*, 42(6), 433–446. <https://doi.org/10.2166/nh.2011.074>
- 822 Staines, J. (2021). *Spatial Relationships Between Trees and Snow in a Cold Regions Montane*
823 *Forest* (Msc Thesis September; pp. 1–121). University of Saskatchewan.
- 824 Staines, J., & Pomeroy, J. W. (2023). Influence of forest canopy structure and wind flow
825 on patterns of sub-canopy snow accumulation in montane needleleaf forests. *Hydrological*
826 *Processes*, 37(10), 1–19. <https://doi.org/10.1002/hyp.15005>
- 827 Storck, P., Lettenmaier, D. P., & Bolton, S. M. (2002). Measurement of snow interception and
828 canopy effects on snow accumulation and melt in a mountainous maritime climate, Oregon,
829 United States. *Water Resources Research*, 38(11), 1–16. <https://doi.org/10.1029/2002wr001281>
- 831 Stull, R. B. (2017). *Practical meteorology: An algebra-based survey of atmospheric science*.
832 (1.02b ed., pp. 1–944). University of British Columbia.
- 833 Thackeray, C. W., Fletcher, C. G., & Derksen, C. (2014). The influence of canopy snow

- 834 parameterizations on snow albedo feedback in boreal forest regions. *Journal of Geophysical*
835 *Research: Atmospheres*, 119(16), 9810–9821. <https://doi.org/10.1002/2014JD021858>
- 836 Vionnet, V., Leroux, N. R., Fortin, V., Abrahamowicz, M., Woolley, G., Mazzotti, G., Gaillard,
837 M., Lafaysse, M., Royer, A., Domine, F., Gauthier, N., Rutter, N., Derksen, C., & Bélair,
838 S. (2025). Enhancing simulations of snowpack properties in land surface models with the
839 Soil, Vegetation and Snow scheme v2.0 (SVS2). *Geoscientific Model Development*, 18(22),
840 9119–9147. <https://doi.org/10.5194/gmd-18-9119-2025>
- 841 Vivioli, D., Kummu, M., Meybeck, M., Kallio, M., & Wada, Y. (2020). Increasing dependence
842 of lowland populations on mountain water resources. *Nature Sustainability*, 3(11), 917–928.
843 <https://doi.org/10.1038/s41893-020-0559-9>
- 844 Wang, L., Cole, J. N. S., Bartlett, P., Verseghy, D., Derksen, C., Brown, R., & von Salzen,
845 K. (2016). Investigating the spread in surface albedo for snow-covered forests in CMIP5
846 models. *Journal of Geophysical Research: Atmospheres*, 121(3), 1104–1119. <https://doi.or>
847 [g/10.1002/2015JD023824](https://doi.org/10.1002/2015JD023824)
- 848 Watanabe, S., & Ozeki, J. (1964). Study of fallen snow on forest trees (II). Experiment on
849 the snow crown of the Japanese cedar. *Japanese Government Forest Experiment Station*
850 *Bulletin*, 169, 121–140.
- 851 Xiao, Q., & McPherson, E. G. (2016). Surface water storage capacity of twenty tree species
852 in Davis, California. *Journal of Environmental Quality*. 45: 188-198, 45, 188–198. <https://doi.org/10.2134/jeq2015.02.0092>
- 854 Zhang, Y., Sherstiukov, A. B., Qian, B., Kokelj, S. V., & Lantz, T. C. (2018). Impacts of
855 snow on soil temperature observed across the circumpolar north. *Environmental Research*
856 *Letters*, 13(4), 044012. <https://doi.org/10.1088/1748-9326/aab1e7>